Spring 2-6-2018

Characterization of wellbore microannuli

Serafin Garcia Fernandez
University of New Mexico

Serafin Garcia Fernandez

Candidate

Civil Engineering

Department

This thesis is approved, and it is acceptable in quality and form for publication:

Approved by the Thesis Committee:

John C. Stormont, PhD, PE Chairperson

Mahmoud Reda Taha, PhD, PEng

Edward Matteo, PhD

CHARACTERIZATION OF WELLBORE MICROANNULI

by

SERAFIN GARCIA FERNANDEZ

B.S., CIVIL ENGINEERING, UNIVERSITY OF GRANADA, SPAIN, 2015

THESIS

Submitted in Partial Fulfillment of the

Requirements for the Degree of

Master of Science

Civil Engineering

The University of New Mexico

Albuquerque, New Mexico

May, 2018

CHARACTERIZATION OF WELLBORE MICROANNULI

by

SERAFIN GARCIA FERNANDEZ

B.S., CIVIL ENGINEERING, UNIVERSITY OF GRANADA, SPAIN, 2015

M.S., CIVIL ENGINEERING, UNIVERSITY OF NEW MEXICO 2018

ABSTRACT

Wellbore integrity is a principal concern for the safe and efficient underground storage of hydrocarbons, disposal of various wastes and in oil and gas production. Poor wellbore integrity can lead to leakage and loss of extracted or stored material, and the potential for contamination of groundwater. The microannuli, which is the space between the steel casing and the cement sheath has been identified as a common and critical leakage pathway. There are no data of the actual size or character of microannuli; however, it is possible to estimate the hydraulic aperture of the microannulus from flow measurements at the wellhead. This information, while providing some insight, could be misleading since it represents the microannuli as uniform annular gap along the wellbore. We created wellbore-shape samples with microannuli between the steel casing and cement and measured gas flow through them to obtain their hydraulic aperture and their permeability.

We injected the microannuli with epoxy after the gas flow measurements, sliced them into five circumferential sections per specimen and measured the microannulus along the steel casing using microphotography. We measured the aperture sizes and the contact between the steel and the cement, creating profiles of the microannulus for each circumferential section. The aperture sizes were fit to different statistical distributions. The capillary entry pressure for CO_2 displacing brine in the microannulus was estimated from the measured aperture size. We found that the capillary entry pressures estimated from the actual aperture sizes were generally much greater than that estimated from the hydraulic aperture of the entire specimen, resulting in a wide range of values, usually far from the interpretation obtained from the flow test. The measured aperture sizes were also used to evaluate the possible repair of the microannulus by estimating the penetration of cementitious materials into the microannulus; we found that the repair is unlikely to be effective for microannuli with a hydraulic aperture less than 50 μm. We conducted a convergence study to estimate how many circumferential sections were necessary to analyze to obtain a representative value of permeability and hydraulic aperture for a specimen.

TABLE OF CONTENTS:

LIST OF FIGURES:

LIST OF TABLES:

LIST OF EQUATIONS:

1. Introduction

Wellbores are constructed for access to the subsurface for a wide variety of purposes, including CO_2 sequestration, hydrocarbon exploration and production, hydrocarbon storage and waste disposal. In the United States alone, over 2.6 million wellbores have been drilled since 1947 (Davies et al., 2014). The most common wellbore configurations comprise a steel casing surrounded by an annular cement sheath. A principal function of the cement is to seal the annular space between the host rock and the casing, thereby limiting fluid communication between the different strata penetrated by the wellbore. In addition, wellbore cement protects the casing from corrosion and provides it with structural support.

Leakage along the wellbore can have serious implications. Confinement of CO_2 within the intended host formation is a fundamental requirement for successful CO_2 sequestration (Zhang and Bachu, 2011). Confinement depends in large part on the hydraulic seal of wellbores associated with these facilities (Bachu and Bennion, 2009; Carey et al., 2007; Zhang and Bachu, 2011). For CO_2 sequestration applications, degradation of the cement from contact with CO_2-rich brines flowing through wellbore systems is a topic of considerable study (Carey et al., 2007; Duguid and Scherer, 2010; Huerta et al., 2009; Kutchko et al., 2007).

In gas production wells, gas is frequently detected at the wellhead, attributable in large part to leakage through the wellbore. In addition to loss of resources, gas leakage can contaminate overlying water-bearing zones and create hazardous surface conditions

(Bielicki et al., 2014; Carroll et al., 2014; Gasda et al., 2004). Wellbore leakage is also an important potential pathway for contamination of groundwater resources by fluids from hydrofracturing operations in underlying gas-bearing strata. Several studies (Jackson et al., 2013; Osborn et al., 2011) found gas contamination in drinking water near hydrofracturing operations, and suggested wellbore leakage was one of the likely causes. Leakage through wellbores can arise from flow through voids or fractures within the cement, along the cement-casing interface, and along the cement-rock interface (Carey et al., 2013; Gasda et al., 2004). Contact between the steel casing and the cement sheath, commonly referred to as the microannulus, has been identified as a common leakage pathway (Bellabarba et al., 2008; Gasda et al., 2004; Huerta et al., 2009). Debonding at the cement-steel interface can arise from cement shrinkage or from temperature and pressure changes within the casing (Bois et al., 2011). The presence of microannuli is widely referred to in the literature (Bellabarba et al., 2008; Dusseault et al., 2014; Gasda et al., 2004; Huerta et al., 2009), although there is little direct information about their nature and size, except that they can be small and still be problematic. Seidel and Greene, (1985) stated that a microannulus of 25 microns was large enough to allow gas flow along the wellbore, and Bachu and Bennion, 2009 observed gas flow in laboratory tests with a microannulus of just 10-15 micrometers.

For the gas to migrate, it has to overcome capillary entry pressure of the fluid filling the pore structure (Checkai, 2012; Dusseault et al., 2014). The capillary entry pressure for one nonwetting fluid such as CO_2 fluid to displace a wetting fluid such as water or brine is directly related to the contact angle, to the size of the pores and to the saturation of the pore (Blunt, 2017). In wellbore integrity, CO_2 storage and enhanced oil recovery there is

interest in finding possible capillary barriers or CO_2 trapping and studying if the gas can migrate through the pore structure (Andrew et al., 2013; Bachu, 2013; Crow et al., 2010; Krevor et al., 2012; Müller, 2011).

Cement bond logs are commonly used in wells to evaluate the quality of the cement behind the casing (Bellabarba et al., 2008; Duguid et al., 2014; Dusseault et al., 2014), including inferring the presence of microannuli. Duguid et al., 2014 interpreted cement bond logs from a 68-year-old well, and found that much of the material behind the casing was unconsolidated cement that did not provide good isolation capacity (Duguid et al., 2014). They interpreted that the microannulus was at least 70 microns by calculating the strain produced in the casing when internal pressure was applied.

Microannulus size can also be estimated from leakage observed through the wellbore. If all of the flow is assumed to occur through the microannulus and it is assumed to be a smooth, open fracture, then the hydraulic aperture of the microannulus is given by the so-called cubic law (Witherspoon et al., 1980)

$$h^3 = \frac{12\ Q\ \mu}{w\ i} \qquad \text{Equation 1}$$

where h is the hydraulic aperture (L), Q is the volumetric flowrate (L^3/T), i is the hydraulic gradient (F/L^3), μ is the fluid viscosity (FT/L^2) and w (L) is the width of the flaw which is assumed to be the outer circumference of the casing. Using this approach, Checkai et al., 2013 interpreted surface-casing vent flow data from 238 wells as

microannulus hydraulic apertures. They found 85% of the apertures ranged from 5 to 100 microns.

Bois et al., 2011 modeled the formation of microannuli in wellbore systems consisting of a cement sheath surrounding a steel casing. The cement was simulated by the modified Cam-Clay model, and the steel was modeled as an elastic material. Their model assumed full contact but no tensile strength between the cement and steel. They demonstrated that cycles of casing pressure can induce plastic behavior in the cement sufficient to produce a microannulus. For the conditions and properties they assumed, they found that increasing the casing pressure to 69 MPa and then reducing it to 0 MPa formed a 29-µm microannulus. The authors concluded that the complicated wellbore system rendered modeling of microannuli difficult at best.

Cement-steel interfaces intended to represent microannuli have been evaluated in laboratory tests. Carey et al., 2010 flowed brine through a steel-cement interface that was then subjected to a confining pressure up to 28 MPa. To permit flow along the interface, they found it necessary to cut grooves into both the cement and the steel. They found corrosion in the steel and an increase in the permeability of the system. They were not able to attribute this to an increase of the microannulus permeability, since they found that the limestone placed right before the cement-steel developed wormholes. In another study (Bachu and Bennion, 2009), the authors created an annular gap between cement and a steel bar, and flowed brine through the gap to study the change in permeability in the samples. They found that just the presence of a microannulus, the presence of radial

cracks, or the combination of both could produce permeabilities up to six orders of magnitude higher than intact cement-steel. For these experiments, the cracks and the microannuli were in the range of 10-300 μm. Boukhelifa et al., 2004 tested samples consisting of an expandable central core surrounded by a cement sheath. Air flow through the cement sheath was measured under a constant confining pressure of 0.3 MPa. Cycles of expansion and contraction of the central core debonded the core from the cement, producing a flow path (i.e., microannulus) along the core-cement contact that increased the system permeability by two orders of magnitude. They interpreted the microannulus width equivalent to the permeability obtained for their specific sample size. By doing so, they showed that with a microannulus just below 20 μm, the permeability could be increased up to three orders of magnitude.

In another analysis, Stormont et al., 2015 tested wellbore samples consisting of a hollow steel casing and a cement sheath under different confining and casing pressures. Specimens that included microannuli between the steel casing and the cement were subjected to confining pressures to 35 MPa and casing pressures to 20 MPa while gas flow was measured through the specimens along the wellbore axis. They interpreted gas flow results in terms of the hydraulic aperture of microannuli as a function of confining pressure and internal pressure for two small (<50 μm) and large (>100 μm) microannuli. Hydraulic apertures were found to decrease non-linearly with increasing stress across the microannuli in a manner similar to fractures in rocks and other materials. In all the laboratory tests described above, the microannuli were characterized in terms of a uniform hydraulic aperture inferred from flow measurements.

Given what is known regarding fractures in cement and rocks, it is unlikely that microannuli have a uniform aperture. Fracture surfaces in cement are rough, and this property is used to obtain information such as fracture toughness and compressive strength (Ficker et al., 2010; Lange et al., 1993). In rock, several studies have attempted to fit the fracture aperture size to different statistical distributions; to date, lognormal is the most popular. Various authors (Bianchi and Snow, 1969; Gale, 1987; Johns et al., 1993) reported lognormal distribution for fractures under different pressures, and (Sanei et al., 2015) used it for both lab and field data. In addition to lognormal, normal (Asadollahi, 2009), gamma (Gentier, 1987) and power law (Barton and Hsieh, 1989; Gale et al., 2007) have been used to describe rock fracture size distributions.

The hydraulic aperture derived from the cubic law deviates from the measured average aperture, presumably due to the roughness of the fracture. The measured aperture is sometimes referred to as the mechanical or actual aperture. Akhavan et al. measured flow through fractured mortar and physically measured the mechanical aperture along the fracture (Akhavan et al., 2012). The mechanical apertures ranged from a few microns to 300 μm, with a mean of 84.8 μm. The hydraulic aperture interpreted from the mechanical aperture was at least twice as large as that obtained from interpreting the flow measurement. This difference is related to the roughness and tortuosity of the fracture. Using published data, (Renshaw, 1995) modified the cubic law on the assumption that the fractures follow a lognormal distribution. He obtained a nonlinear relation between the hydraulic and the mechanical aperture. When (Hakami and Larsson, 1996) estimated the hydraulic aperture of a rough rock fracture from flow tests using the cubic law and

measured the actual aperture after injecting epoxy into the fracture, they found that the mean mechanical aperture was 360 μm and the hydraulic aperture interpreted was 250 μm. These studies highlight the concept that the hydraulic aperture derived from flow measurements does not provide a direct measure of the actual (or mechanical) aperture of a microannulus and offers no information about its spatial variability.

In the same way that information regarding aperture distribution is important to understanding the mechanical and hydrologic response of rock fractures (Patir and Cheng, 1978; Renshaw, 1995; Witherspoon et al., 1980), micronannulus response to changes in stress and/or temperature will be affected by the aperture distribution. In addition, the penetration of material to repair the microannulus (e.g., microfine cement) depends on the actual aperture size, not a single value average such as the hydraulic aperture. There is thus a need to understand the microannulus aperture distribution. To this end, we measured mechanical aperture distribution of microannuli at casing-cement interfaces, and compared these results to the hydraulic apertures interpreted from flow measurements on these microannuli using the cubic law.

2. Materials and methods

2.1 Wellbore specimen preparation

Specimens of a hollow steel casing surrounded by a cement sheath were constructed to simulate a wellbore configuration. The casing is carbon steel with an outer diameter of 60 mm and a thickness of 2.35 mm. Cement proportions for the specimens were 1000 g API class G cement, 330 g distilled water, 100 g silica fume and 6.6 g plasticizer. Typically, the water to binder ratio used for wellbore cement is 0.45 (API, 2009) and no additives are required. For our wellbore specimens we used a 0.3 water to binder ratio and we added silica fume (0.1 silica fume/cement). Before setting a W/C ratio of 0.3, several wellbore specimens were produced using different W/C ratios. We opted for 0.3 W/C ratio because we found that higher ratios produced bleeding in the cement.

At the beginning of this research wellbore specimens did not have silica fume. We added it to add strength to the specimens. Before having silica fume, the specimens broke often when the pressure was increased in during the tests performed, especially when applying casing pressure. Silica fume (SiO_3) reacts with the calcium hydroxide (CH) forming calcium-silicate-hydrate (CSH), which is a strong bond that increases the strength of the cement.

The cement was prepared following the ASTM C305 – 14 (ASTM, 2014). The cement was cast around the steel in PVC molds. After 24 hours, samples were unmolded and

placed in a curing room for 28 days (100% humidity, 24°C). Specimens were 185 mm long and the cement sheath was 30 mm thick.

Figure 1. Finished wellbore-shape specimen, comprised of a steel casing and a cement sheath.

Three wellbore specimens which included a microannulus between the cement and casing were used in this study. Two different techniques were used to create the microannulus. For specimens with a relatively large aperture, the steel casing was wrapped with a thin (25 µm) plastic release film and the cement was cast around it. After 24 hours, the casing was pulled from the cement sheath, the film removed, the casing reinserted into the cement sheath, and the specimen was cured for an additional 27 days. Subsequent gas

flow testing of samples with microannuli formed by this method indicated hydraulic apertures were greater than 50 μm. To create microannuli with smaller apertures (hydraulic apertures less than 50 μm), the steel casing was thermally debonded from the cement. Dry ice (-79 ºC) was placed inside the casing of a cured specimen and both ends of the steel casing were tapped with a rubber plug to preserve the temperature. After 5 minutes, the dry ice was removed and warm water (40 ºC) was added for another 5 minutes. The low temperature contracts the casing, pulling it apart from the cement, and the elevated temperature expands the casing. The process was repeated 4 times to ensure debonding.

Wellbore specimens A and B apertures were generated with the release film method, and the thermal debonding method was used to generate the aperture of specimen C.

2.2 Gas flow measurements

Gas flow measurements were measured to characterize the microannulus. Specimens were placed in a steel pressure vessel and subjected to hydrostatic stress conditions. Gas flow measurements were made along the axis of the samples and thus included the microannulus. The test system is shown in Figure 2.

The pressure vessel was capable of applying independent confining and casing pressure up to 35 MPa and 20 MPa, respectively. Confining pressure was regulated through a port on the side of the pressure vessel. Hydraulic oil was pumped, changing the pressure applied to a flexible membrane that was in contact with the cement sheath.

Casing pressure was regulated through the end caps of the pressure vessel. A port in the center of the end caps allowed connection of a hydraulic pump to the interior of the steel casing. Both end caps fitted tightly into the steel casing, which isolated it.

An additional port in the end caps was used to perform gas flow experiments. Gas was introduced into the pressure vessel using the upstream port and flowed through the cement sheath and the steel-cement interface. Steady-state flow rates were measured using flowmeters (from 5 to 150 standard cm^3/s, full-scale of the flowmeter) with an accuracy of 1% of full-scale connected to the downstream port. The gas pressured applied was read using a pressure gauge before the upstream port.

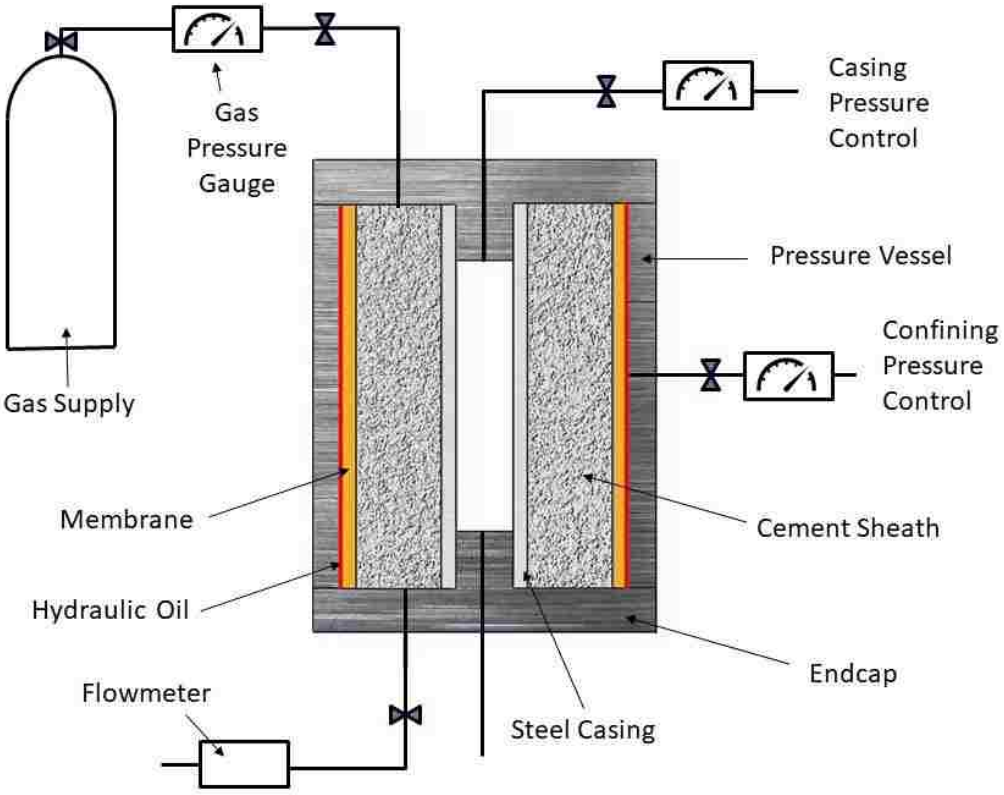

Figure 2. Scheme of the pressure vessel system used to test the wellbore specimens.

Permeability was interpreted from the gas flow measurements using Darcy's law.

$$k = -\frac{Q\mu}{A}\nabla \mathrm{P} \qquad \text{Equation 2}$$

Where *k* is the permeability, *Q* the volumetric flow rate, *A* the cross-sectional area involved in the flow, ∇P the pressure gradient and μ the viscosity of the gas used.

Darcy's law states that the flux changes linearly with the change in pressure difference. With the test conditions used, non-linear or inertial flow often occurred. In these conditions, the flux varied non-linearly with the pressure gradient and the flow could be described by the Forchheimer equation (Forchheimer, 1901):

$$\nabla P = -\frac{\mu}{\mathrm{k}A}Q + \frac{\beta\rho}{A^2}Q^2 \qquad \text{Equation 3}$$

which is Darcy's law plus a term to account for the non-linearity. β is the inertial coefficient and ρ is the density of the gas. This equation can be rewritten as:

$$\frac{MA(\mathrm{p}_1^2 - \mathrm{p}_2^2)}{2\,z\,R\,T\,\mu\,l\,\rho\,Q} = -\frac{1}{\mathrm{k}} + \beta\,\frac{Q\,\rho}{\mu \mathrm{A}} \qquad \text{Equation 4}$$

where M is the molecular weight of the gas, R the universal gas constant, p_1 the upstream pressure, p_2 the downstream pressure, z the compressibility factor of the gas, *l* the length of the sample and the gas is assumed to be ideal. Plotting the x, y terms for a series of measurements allow both *k* (interpreted) and β (slope) to be found. Thus, the equation is of the form:

$$y = \frac{1}{k} + \beta x \qquad \text{Equation 5}$$

To allow correction for inertial flow, a series of flow rates were measured as a function of the gradient. The gradient was changed by adjusting pressures on the upstream and downstream sides of the specimen). From the plotted data, the inertial coefficient β is obtained as the slope of the straight line and the inverse of the permeability is the intersection of the straight line with the y axis (figure 3) If there is no nonlinear flow, β is 0 and Darcy's equation is valid.

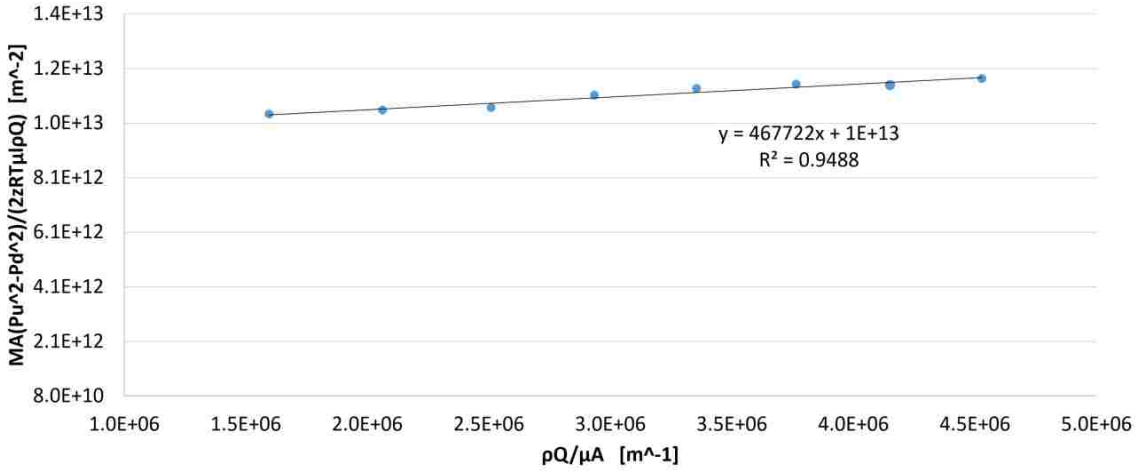

Figure 3. Forchheimer's correction for non-linear flow in wellbore specimen C.

Once the corrected permeability value is obtained at the specific stress state, the cubic law (equation 6) is used to interpret this permeability as a hydraulic aperture. It is assumed that the entire flow passes through the microannuli. This assumption is based on our experimental data; microannulus have a transmissivity orders of magnitude higher than the intact cement. Another assumption is that the flow between two parallel plates is equivalent to the flow between two concentric cylinders. This is done under the premise that, if we take infinitesimally small portions of the microannuli along the circumferential

section and estimate individually the flow through them, the error produced while doing that could be negligible (Stormont et al., 2018).

Therefore, the equation used was:

$$h^3 = \frac{12kA}{w} \qquad \text{Equation 6}$$

where h is the hydraulic aperture, k is the permeability of the wellbore system estimated from the observed leakage using Forchheimer's correction, A cross-sectional area of the entire specimen and w is the width of the microannulus. In this case, w is the circumference of the outer diameter of the steel casing.

2.3 Specimen preparation for image analysis

Novolac epoxy was injected in the microannulus for its characterization after the specimen was removed from the pressure vessel at the conclusion of the gas flow measurements. Novolac is a two-component epoxy mixed at a 2.2:1 resin-hardener ratio. The resin is a mixture of Novolac backbones with epichlorohydrin epoxy resin including silane. The hardener is diethylenetriamine (DETA), phenol, 4,4'-(1-methylethylidene)bis-, and tetraethylenepentamine. Rhodamine B was added (0.1% of the epoxy weight) to epoxy to yield bright pink fluorescence, which aided microannulus characterization by improving the epoxy contrast with the cement and the steel.

To prepare for the injection, samples were placed into 101.6 mm PVC molds and epoxy was poured to surround the sample to ensure the sealing between the specimen and the PVC mold; hence the only flowpath available for the epoxy to flow is the microannuli. In addition, it assures the integrity of the cement during the cutting later. Rubber caps were placed inside the hollow steel casing, thus the only flow path available for epoxy with rhodamine B was the microannulus (Figure 4).

Figure 4. Wellbore specimen inside the PVC mold with the surrounding epoxy and the rubber plug, ready to pour the epoxy over it and place the specimen in the injection system.

The epoxy-rhodamine B preparation was poured over the top surface of the sample, which was placed in the injection setup (F

Figure 5). The setup was comprised of two plastic endcaps with O-rings to seal the space between the mold and the endcaps. They sit atop another PVC mold that acts as a stabilizer. The steel frame prevents movement of the top endcap and holds the pieces together. Air pressure (65kPa) was applied through the top endcap to “squeeze” the epoxy into the microannulus.

Figure 5. Injection setup used to inject the microannuli with epoxy.

After injection, some epoxy was visible on the bottom of the sample (see Figure 6), which indicated that epoxy travelled through the length of the specimen along the microannulus.

Figure 6. Bottom of a sample after injection, which shows that the epoxy entered the microannulus at the top, flowed through and came out of the bottom.

Once injected, the epoxy cured for a week and then samples were sectioned horizontally and polished to remove imperfections. A MK Diamond Producs, Inc. brick saw, equipped with a 355.6 mm-diameter, 3.5-mm thick concrete blade was used to section the samples (Figure 7). Samples were held in a vise and two wood paint sticks were used as cushion between the sample and the vise.

The sectioned sample was polished with a belt sander. Progressively finer sandpaper was used (grit sizes from 50 to 120). It was necessary to polish the sample from casing outward to preserve the microannuli and so that the cement was not smeared over the microannulus.

The injection of the microannuli with dyed epoxy was made outside the pressure vessel without confining pressure. On the other hand, the flow tests performed to characterize

the microannuli with a hydraulic aperture were conducted with a nominal confining pressure. The nominal confining pressure was applied so it was ensured that there was no gas flowing between the specimens and the bladder. Ideally, the injection of the specimen should be done under the same conditions as the flow tests were performed. Injecting inside the pressure vessel entails several technical difficulties; the most important is that once the epoxy sets it is practically impossible to remove, therefore potentially ruining components of the pressure vessel including end caps and pressure lines. For that reason, we opted for injecting outside the pressure vessel in a secondary system.

Figure 7. An MK brick saw with vise and wood cushions was the sectioning setup used.

For specimen nomenclature, the first letter refers to the specimen (A, B or C), followed by a digit that indicates the position of the specific circumferential section in the sample (1, top, to 5, bottom) as shown in Figure 8. This is followed by a letter that defines the

face of the piece (a, top face; b, bottom). For instance, A.3.a is the top face of the cross section labeled as 3 of wellbore specimen A (Figure 8).

Figure 8. Wellbore specimen A sectioned, with all the circumferential sections labeled.

2.4 Image Analysis

Photographs were taken along the circumference of the steel casing to describe the aperture size and distribution. Photographs of wellbore specimen A and B were taken with an usb camera with 5 MegaPixels (MP) using x100 magnification. The resolution was 3 µm. Photographs of specimen C were taken with an usb 5 MP camera and x220 magnification. The higher magnification was needed to accurately measure the small apertures in this specimen. The resolution was 0.4 µm.

For specimen C, we constructed an automated rotating photography system setup (Figure 9). A servo motor was attached to a mount that fit into the steel casing of the sectioned sample and, controlled by an Arduino Uno R3 Microcontroller, was set to rotate 1.5 degrees and stop for 5 seconds. The camera automatically acquired an image while the sample was not moving.

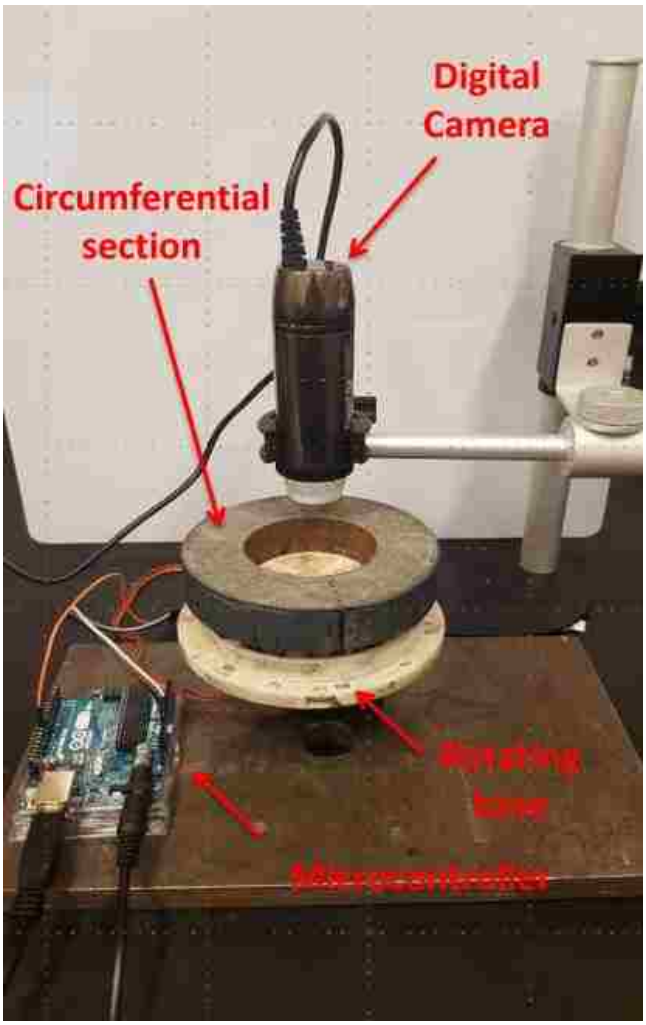

Figure 9. Automated rotating photographic system, comprised by a servo motor controlled by an Arduino board and a servo motor.

For accurate measurement and to avoid miscalculation due to overlap, automated image merge was performed using the built-in Adobe Photoshop 2014 photomerge function (Figure 10). This function becomes more computationally expensive as the number of photographs increases, since it gathers all photographs simultaneously and attempts to find matching parts. The function worked efficiently with circumferential sections of specimens A and B, but for the specimen C (with twenty times as many images per

circumferential section), computational time increased substantially and errors were more frequent. A script was therefore generated that used the built-in photomerge function, but changed the number of images the software processed simultaneously. When the script was launched, it opened two consecutive images, merged them and saved the result. When all merges had been executed, it picked the results from the previous merge, always two at a time, and merged them again, finally generating a single image, which is the merge of all the original images. For example, for four consecutive photographs, for the photomerge function, Photoshop opens all four simultaneously and attempts to identify the pixels that contain the same information. Using our script, Photoshop first opens photographs 1 and 2, merges and saves them as image 2.0. It then opens images 3 and 4, merges saves them as image 2.1; finally, it opens image 2.0 and 2.1 and merges them.

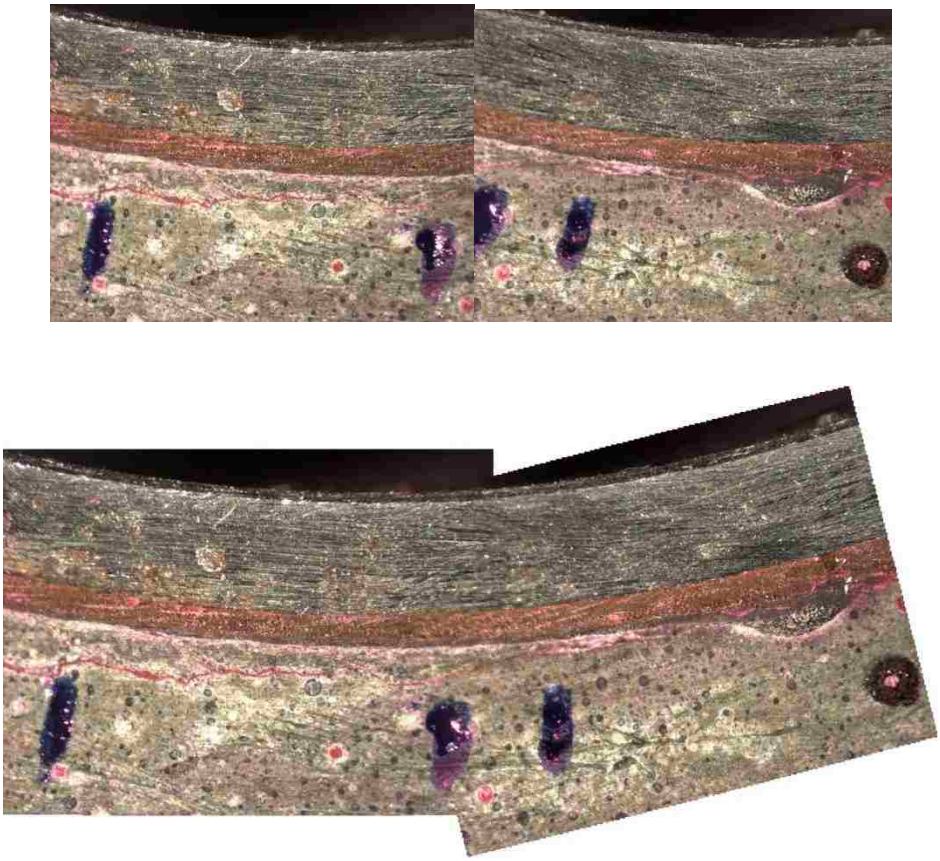

Figure 10. Example of the merge of two consecutive images done using Photoshop function "photomerge".

X-ray CT have been used to study interfaces between materials (Crandall et al., 2010; Deng et al., 2013), to measure fracture apertures (Johns et al., 1993) and to measure porosity and saturation (Bertels et al., 2001; Krevor et al., 2012). These techniques offer advantages over cutting the specimen and looking at it using microphotography. CT scan and X-rays are non-destructive techniques and provide many experimental possibilities. In addition, non-destructive techniques allow more frequent measurements along the casing axis than the cutting method that we used. However, resolving very small apertures was crucial for achieving our objectives and microphotography provided a

significantly better resolution compared to CT scan and X-rays; 27.4 µm x 27.4 µm the CT scan (Crandall et al., 2010) compared to 0.4 µm x 0.4µm that the microphotography provided.

2.4.1 Aperture measurement

After photograph merger, ImageJ software (National Institutes of Health, Bethesda, MD) was used for the remainder of the processing. The merge was split into smaller sections of equal width (represented as "w" in Figure 11). The fluorescent rhodamine B in the epoxy served as a tracer of the filled microannulus, which allowed us to establish a color threshold to select the microannulus color. The ImageJ function "Analyze particle" was used to measure the area (in pixels) within the threshold, which provided a precise measurement of the microannulus area. Dividing this area by the width of the split photograph yielded an average height of the microannulus for each section.

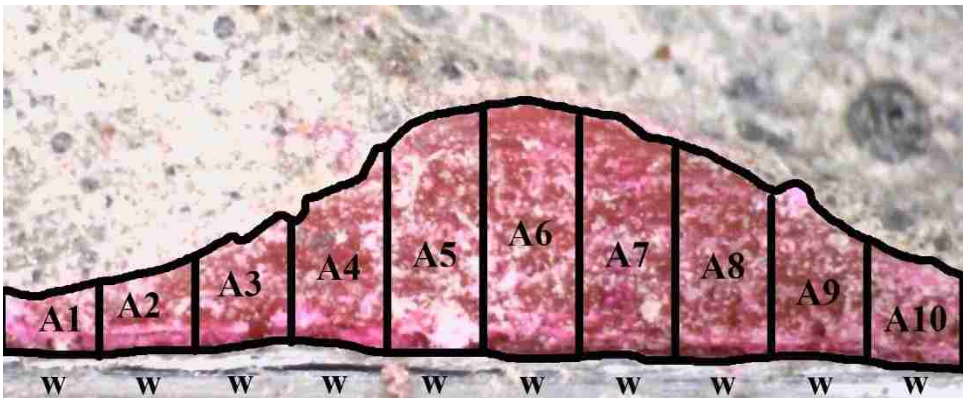

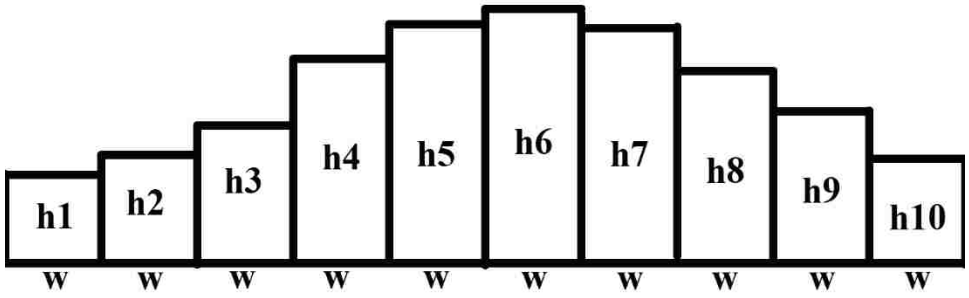

Figure 11. Interpretation of the apertures. The areas measured over constant widths "w" (A1, A2, A3…) are divided by w to obtain height measurements (h1, h2, h3…). The aperture is interpreted as different heights, spaced at constant w.

Wellbore specimens A and B were split in 360 equal sections and C was split in 7200 equal sections of width w. The value of "w" was 510 µm for specimens A and B, and 25 µm for C. Wellbore specimen C was split in smaller "w" than A and B because the aperture width was considerably smaller and less continuous.

All the apertures found in wellbore specimen C had a width of at least 25 µm; this lead to the use of splits ("w") of this size. A smaller "w" could have been used too, but the analysis would have become more computationally expensive since it would have increased the number of areas to measure and there was no indication that the hydraulic aperture results were going to be significantly better. On the other hand, if we had chosen splits larger than 25 µm we would have underestimated some apertures size. This can be explained easily with an example. Assume an isolated aperture of height 50 µm and a width of 25 µm. If the splits are done every 25 µm, one split will capture all the aperture

and the precedent and following splits will represent no aperture, which is a realistic representation of the aperture and the contact in the specimen. If we had chosen a "w" of 50 μm, the aperture and some contact will be averaged in one split, representing a continuous aperture of 50 μm with a height of 25 μm. While the total area represented in both cases is the same, the latter will result in a lower transmissivity of the fracture because the height of the aperture is what controls the flow; this is a consequence of interpreting the height from an area. If the aperture width is smaller than the "w" used, the area measured following the above procedure would be interpreted as a unique "h" value, and not as contact between steel and cement (no aperture), followed by a higher "h" than that estimated.

2.4.2 Information obtained from this analysis

Aperture size was obtained over the circumference of the samples using the method indicated above. To describe each surface, we calculated contact percentage, average mechanical aperture and hydraulic aperture from the measured data.

Contact is defined as the absence of aperture. Contact percentage is the number of splits with no area divided by the number of measurements made (360 for specimen A and B, 7200 for specimen C). Average mechanical aperture is sum of the mechanical apertures for each measurement divided by total non-zero measurements. The hydraulic aperture is obtained from the cubic law using the equation:

$$Hydraulic\ aperture = \frac{\sum_{i=1}^{n} \sqrt[3]{(\mathrm{w_i} * {h_i}^3)}}{\sum_{i=1}^{n} w_i}$$ Equation 7

where w is the width of the measurement, which is constant in all measurements, h is the measure of aperture, and casing circumference length is the sum of all w.

3. Results and discussion

Microphotographs of cement-steel contact in sliced circumferential sections revealed a wide range of geometric characteristics for microannuli (sizes and shapes); Figure 1 shows microphotographs illustrating typical characteristics. The observed aperture size varied from a few microns to nearly 1 mm (Figure 1a, b). The aperture could be uniform over the circumferential arc of a microphotograph (Figure 1c) or could show significant variability (Figure 1d). In some cases, isolated channels were observed (Figure 1e). A portion of every circumferential section had perfect contact, that is, there was no detectable aperture and therefore no microannulus (Figure 1f).

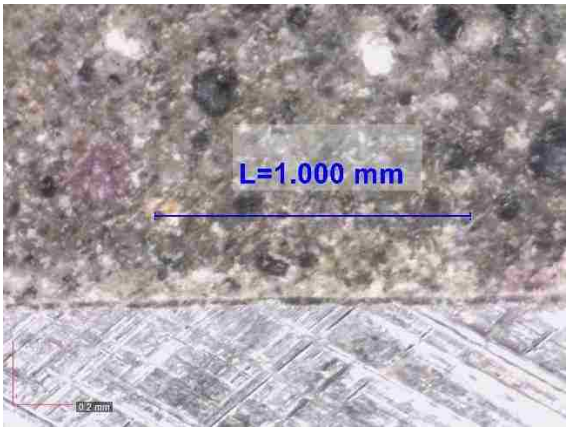

a)

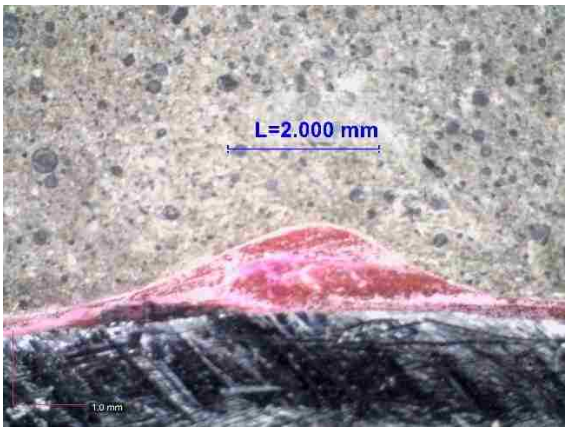

b)

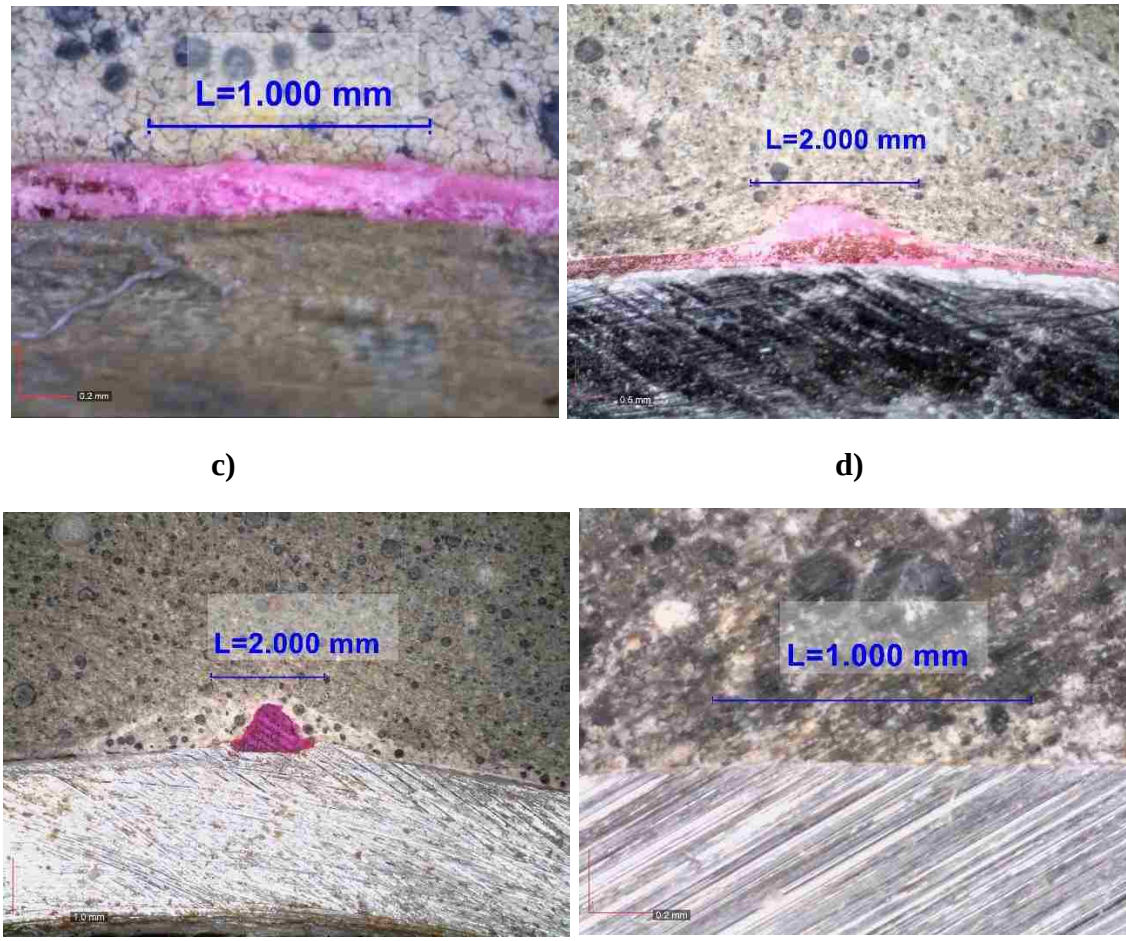

Figure 12. Different geometries observed in the microannuli. a) Small continuous aperture (35 µm) in wellbore specimen C. b) Big aperture (1140 µm) found in wellbore specimen A. c) Uniform and continuous aperture (185 µm) in wellbore specimen B. d). Variability in the aperture size found in wellbore specimen A, where the aperture changes from 230 µm to 760 µm and then back to 196 µm. over a distance of 2mm. e) Big channel (865 µm), preceded and followed by perfect contact in wellbore specimen B. f) perfect contact between the steel and the cement, which indicates the absence of microannulus. (wellbore specimen C).

The measured aperture size around the circumference of one circumferential section for each wellbore specimen is shown in Figure 13, Figure 14 and Figure 15. The horizontal distance starts at an arbitrary point and goes around the steel casing.

Because of the large number of measurements made on each section of sample C, it was necessary to provide these data in four figures in order for the individual measured values to be resolved in the figures.

The aperture data are shown as cumulative distribution functions in Figure 16; they provide an indication of the spatial variability of the aperture size for each section as well as differences between samples. The section from Sample A has a wide range of apertures that can vary significantly over small distances. The section from Sample B reveals more contact (no aperture) compared with Sample A and discrete regions or channels with relatively large, non-uniform apertures. The section from Sample C reveals consistently small apertures: 90% of the non-zero measurements were below 10 μm and only 2 of the 7200 (including 0s) individual measurements over 30 μm.

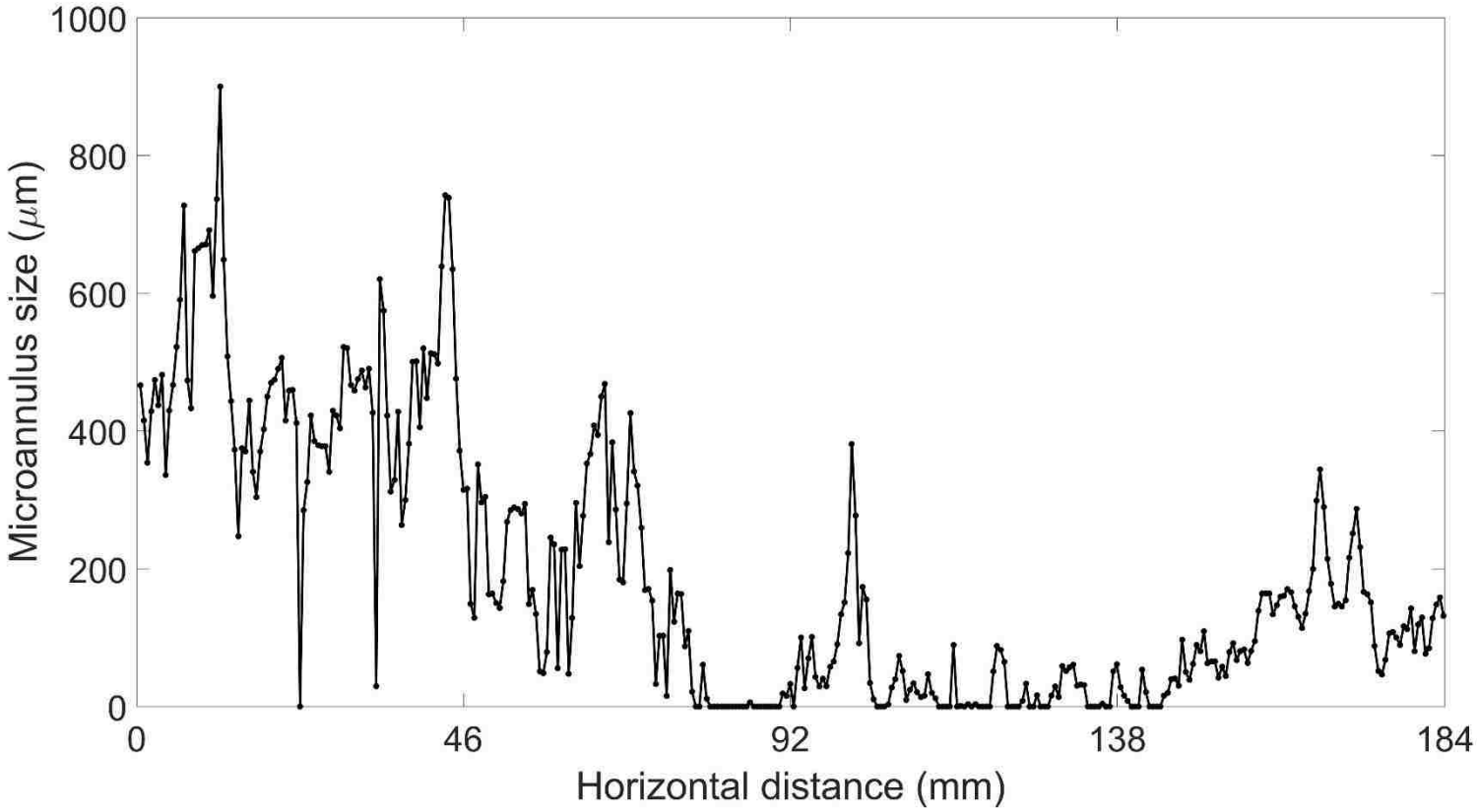

Figure 13. Aperture in the upper wellbore specimen A (A.2.b). The Y axis represents the aperture measured and the X axis represents the horizontal distance between the measurements.

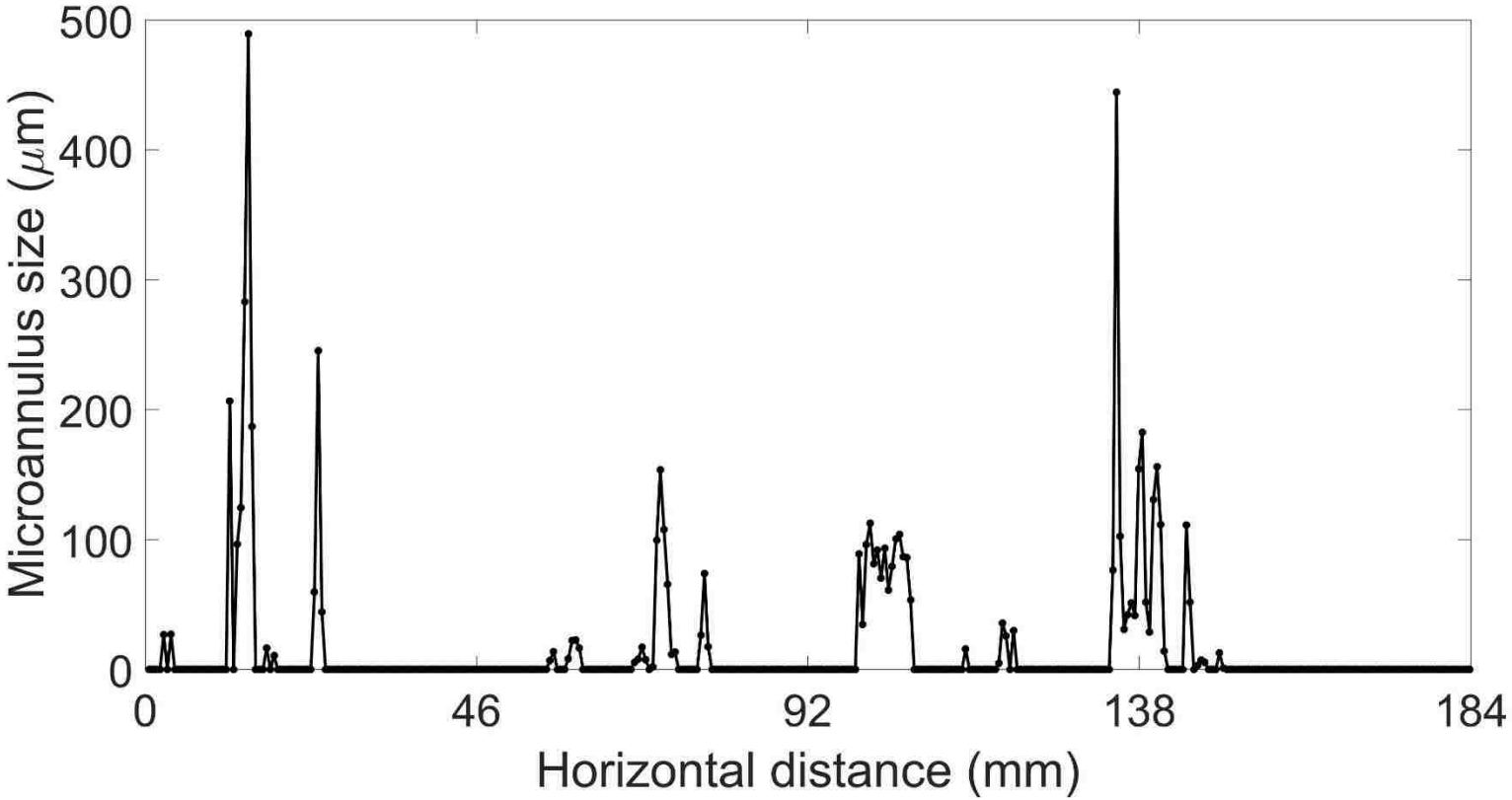

Figure 14. Microannulus in the upper wellbore specimen B (B.2.b). Each point represents a measurement. The Y axis represents the aperture measured and the X axis represents the horizontal distance between the measurements.

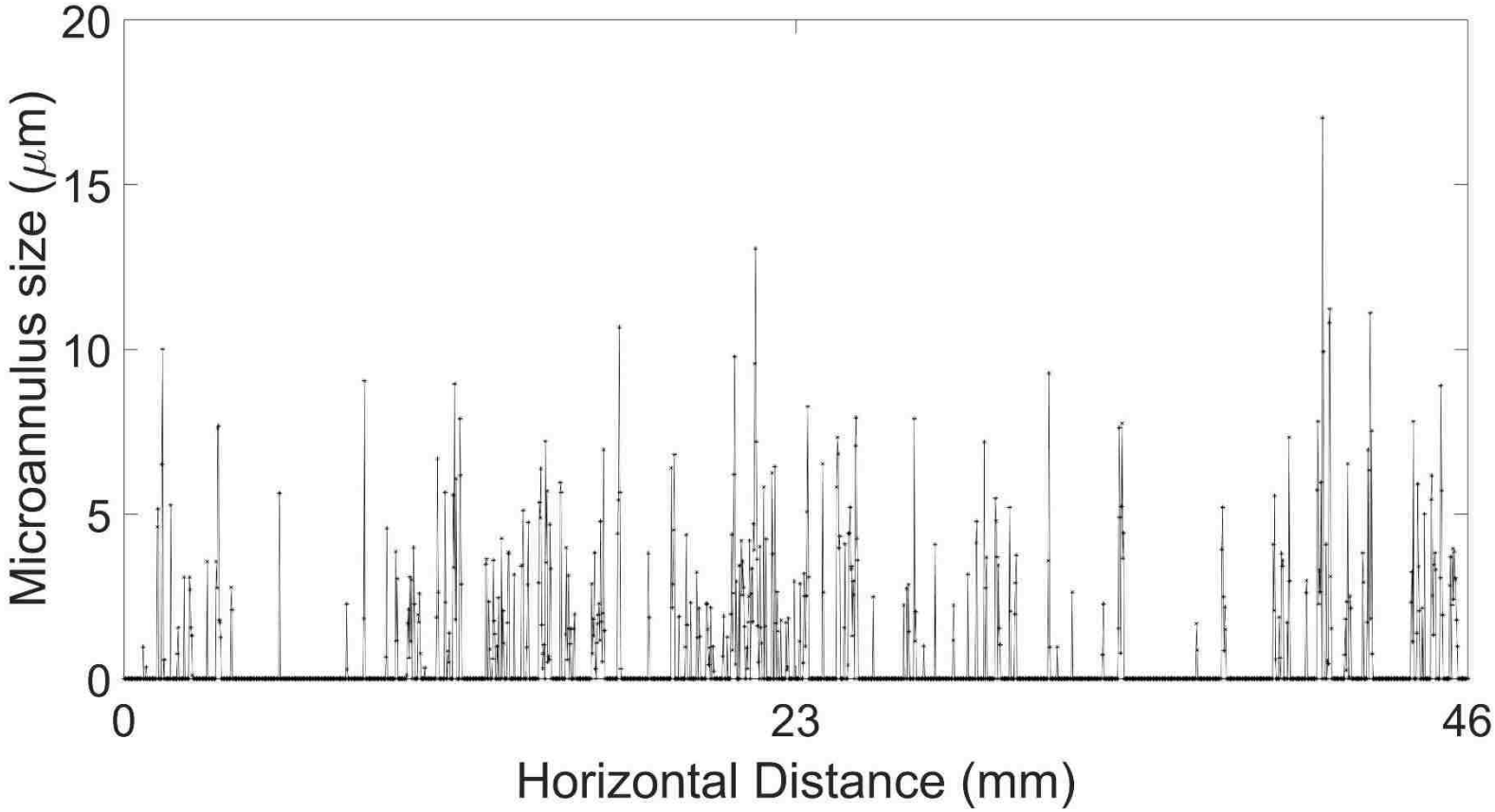
20
15
10
5
0
Microannulus size (μm)
0
23
46
Horizontal Distance (mm)

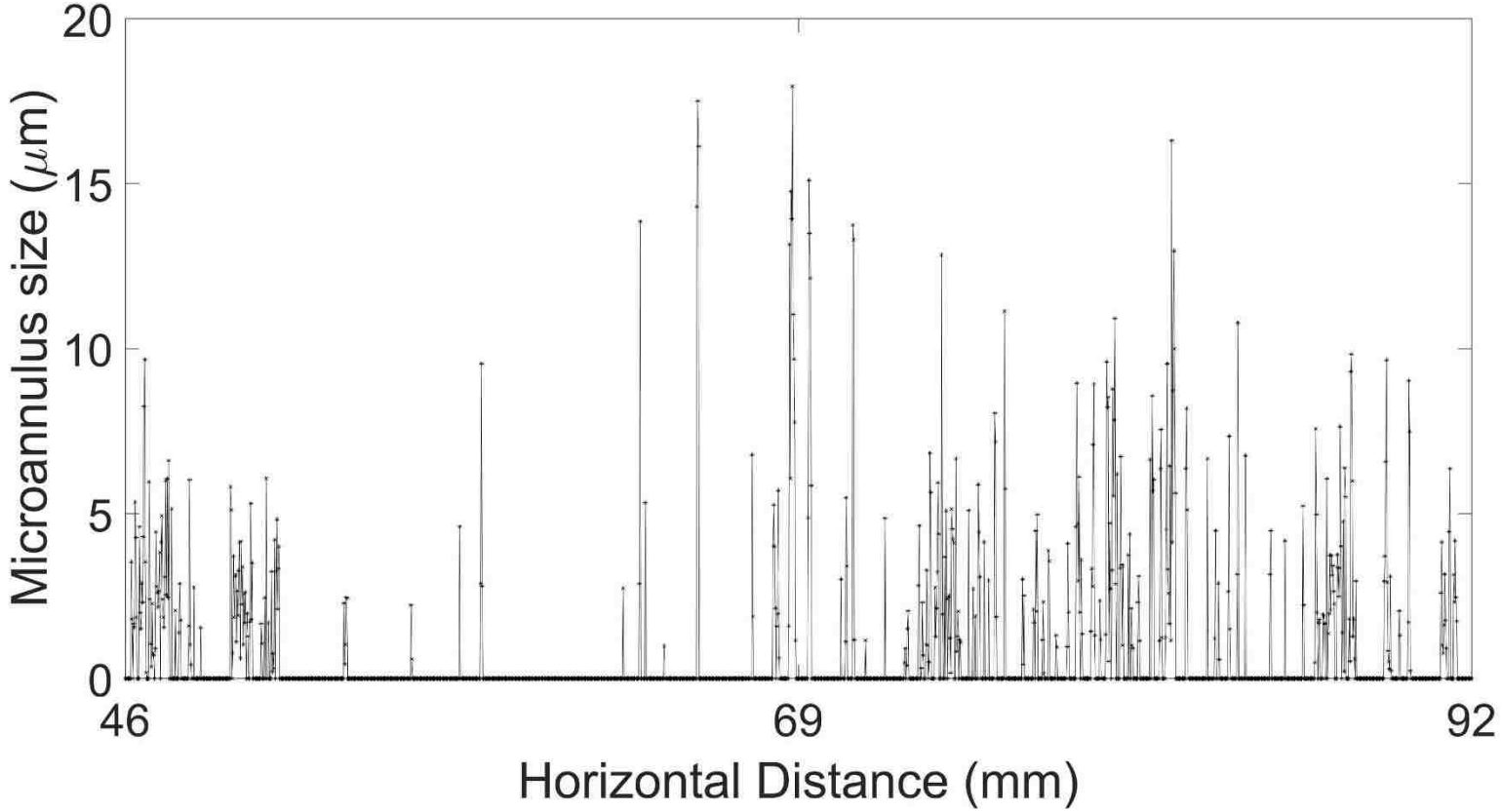
20
15
10
5
0
Microannulus size (μm)
46
69
92
Horizontal Distance (mm)

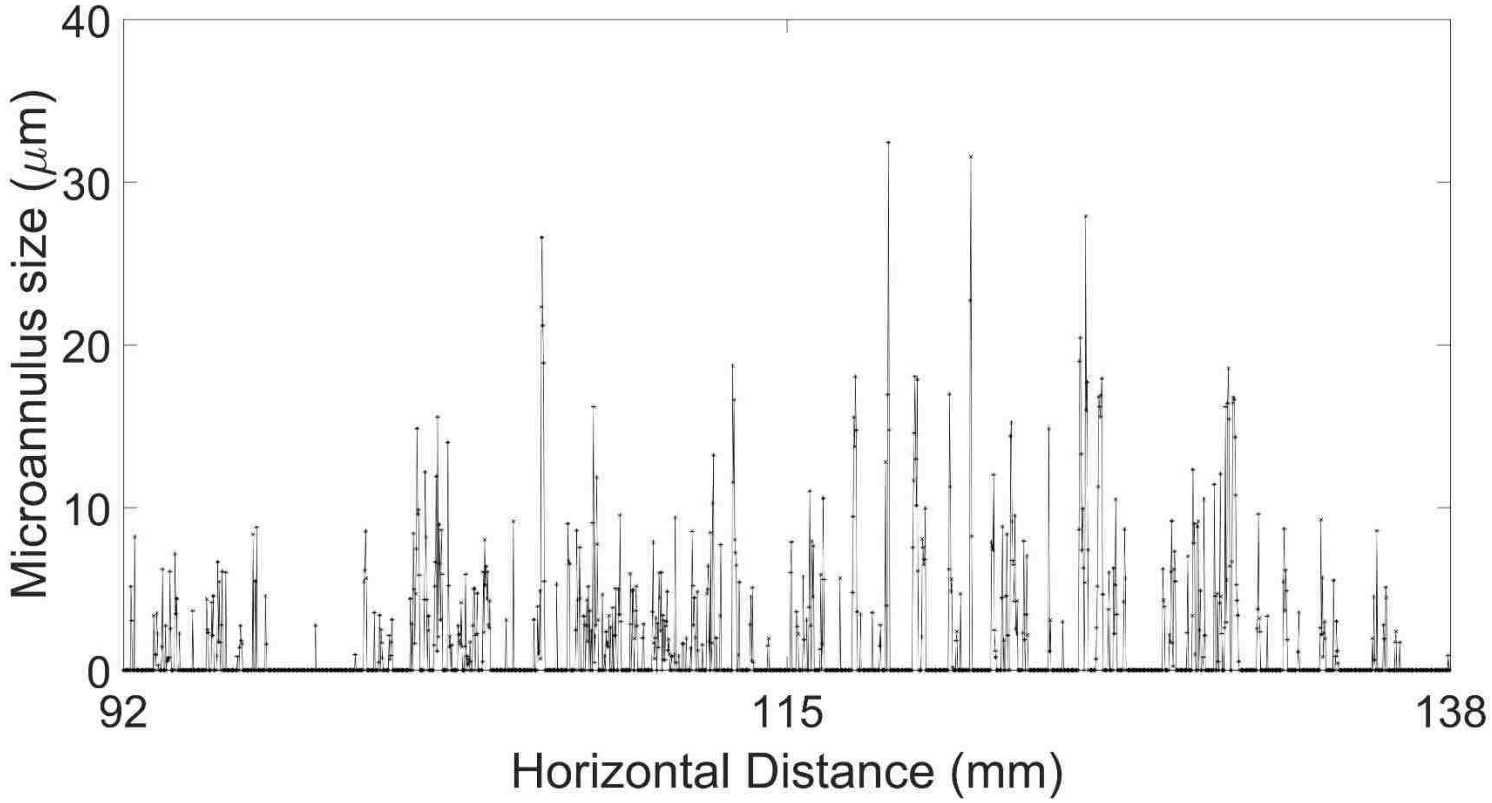
40
30
20
10
0
Microannulus size (μm)
92
115
138
Horizontal Distance (mm)

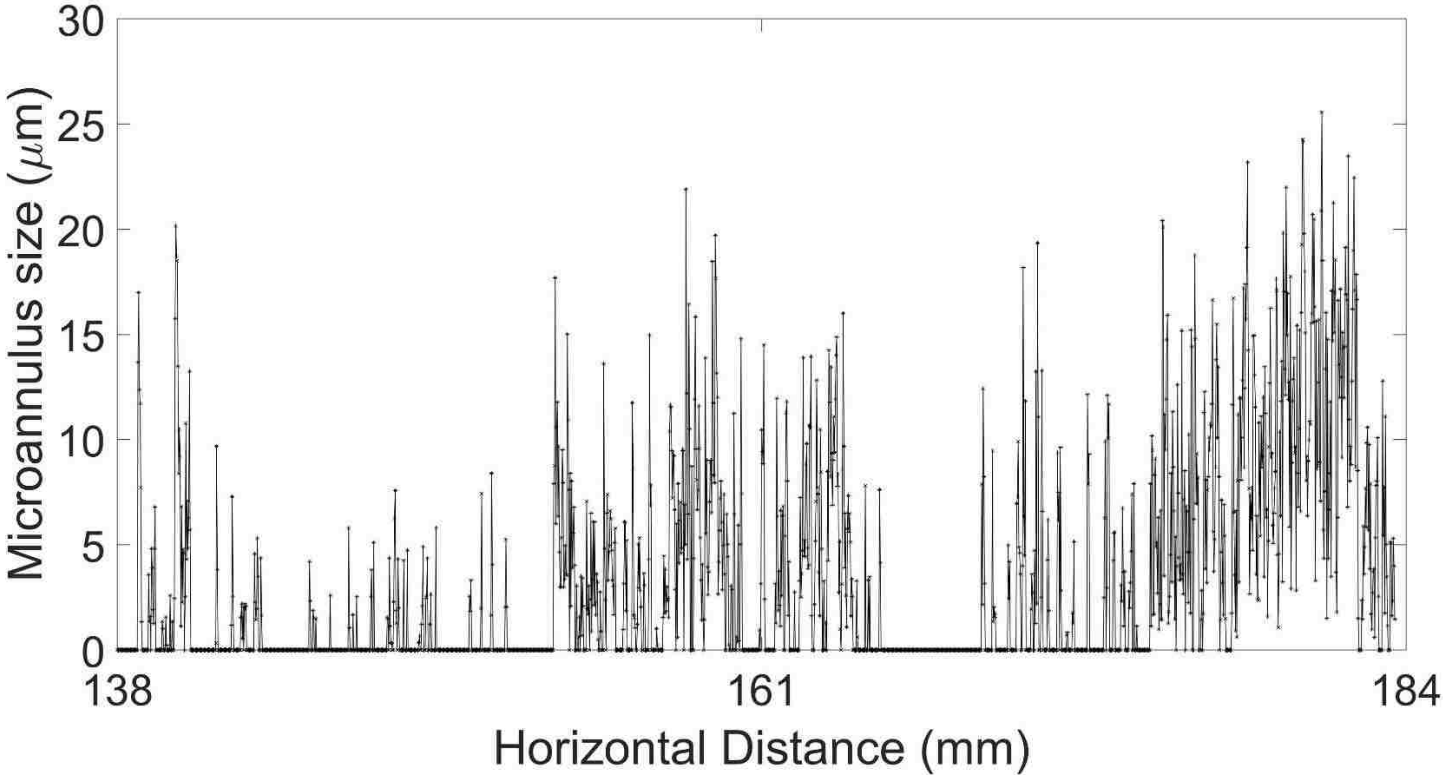

Figure 15. Microannulus near the lower part of sample C (C.4.b). Each point represents a measurement. The graph was split into four parts to represent in a bigger detail the 7200 measurements of this circumferential section. The Y axis represents the aperture measured and the X axis represents the distance between the measurements.

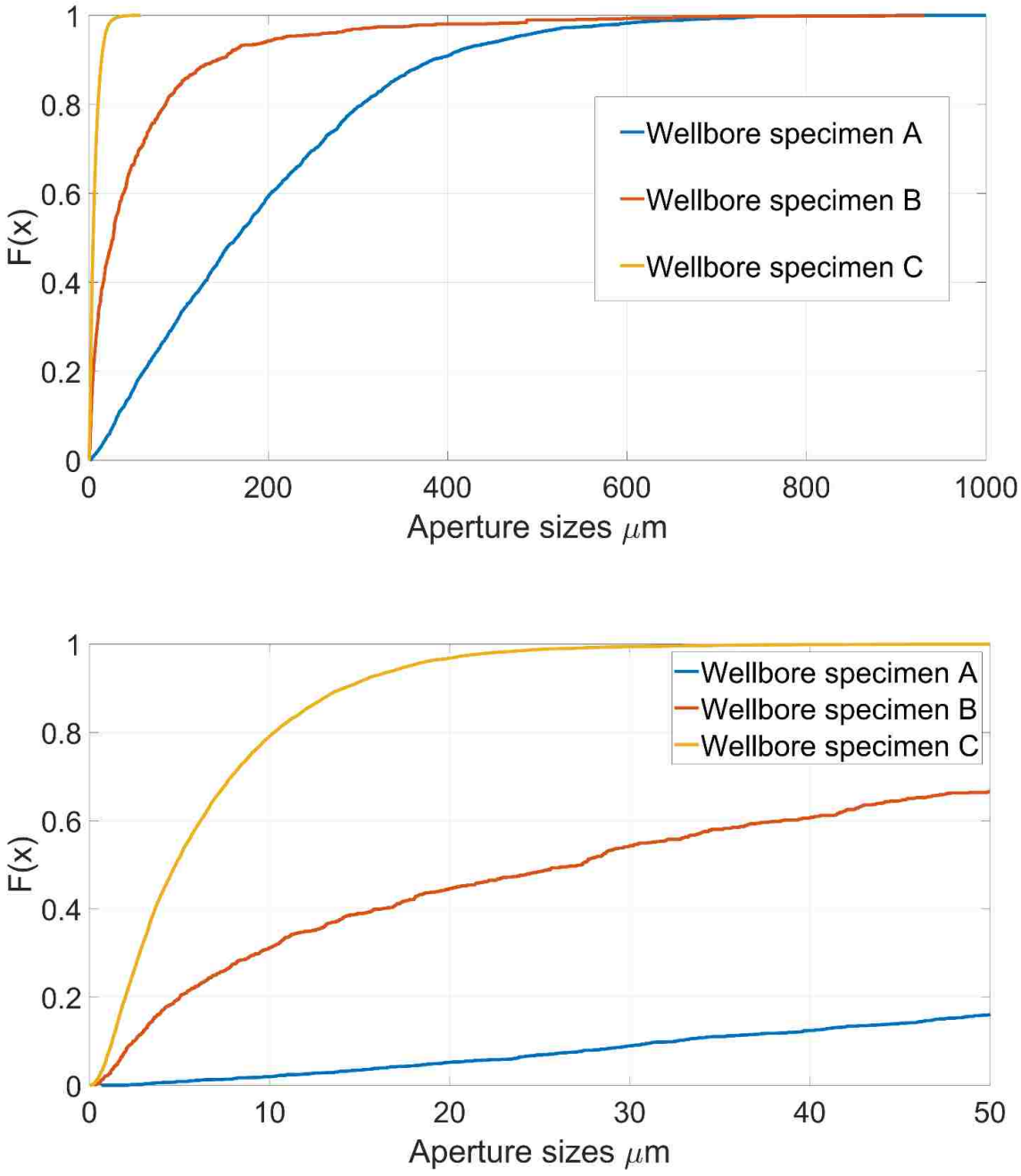

Figure 16. A) Cumulative distribution function of the wellbore specimens A, B and C. B) Cumulative distribution function of the wellbore specimens A, B and C zoomed at the range 0-50 µm to show in detail wellbore specimen C

The aperture size for the entire sample is given as a three-dimensional (3D) plot in Figure 17, Figure 18 and Figure 19 for wellbore specimens A, B and C, respectively. In these figures, the cylindrical cement-steel contact has been "unrolled" and is shown as a plane. In both the circumferential and longitudinal directions, linear interpolation is used to recreate the surface between adjacent measured points. These plots provide a means to visualize the microannulus and illustrate aperture variability within a specimen as well as between samples.

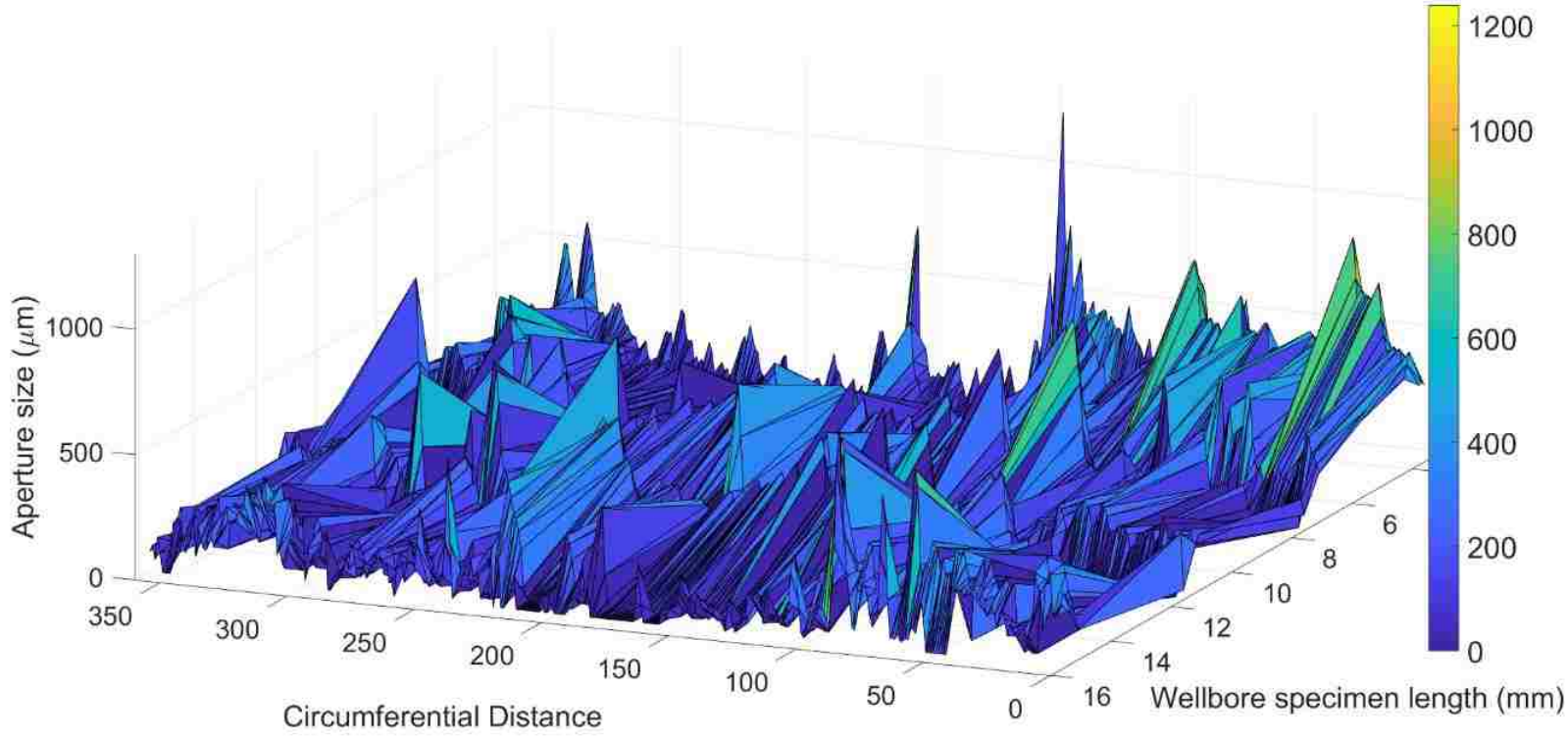

Figure 17. 3D plot of circumferential section of wellbore specimen A. The X axis is the distance between two consecutive measurements (circumferential distance), which is the value "w" already explained, and is a measurement every degree. They Y axis is the aperture size measured in microns and the Z axis represents the position in the specimen of each circumferential section measured.

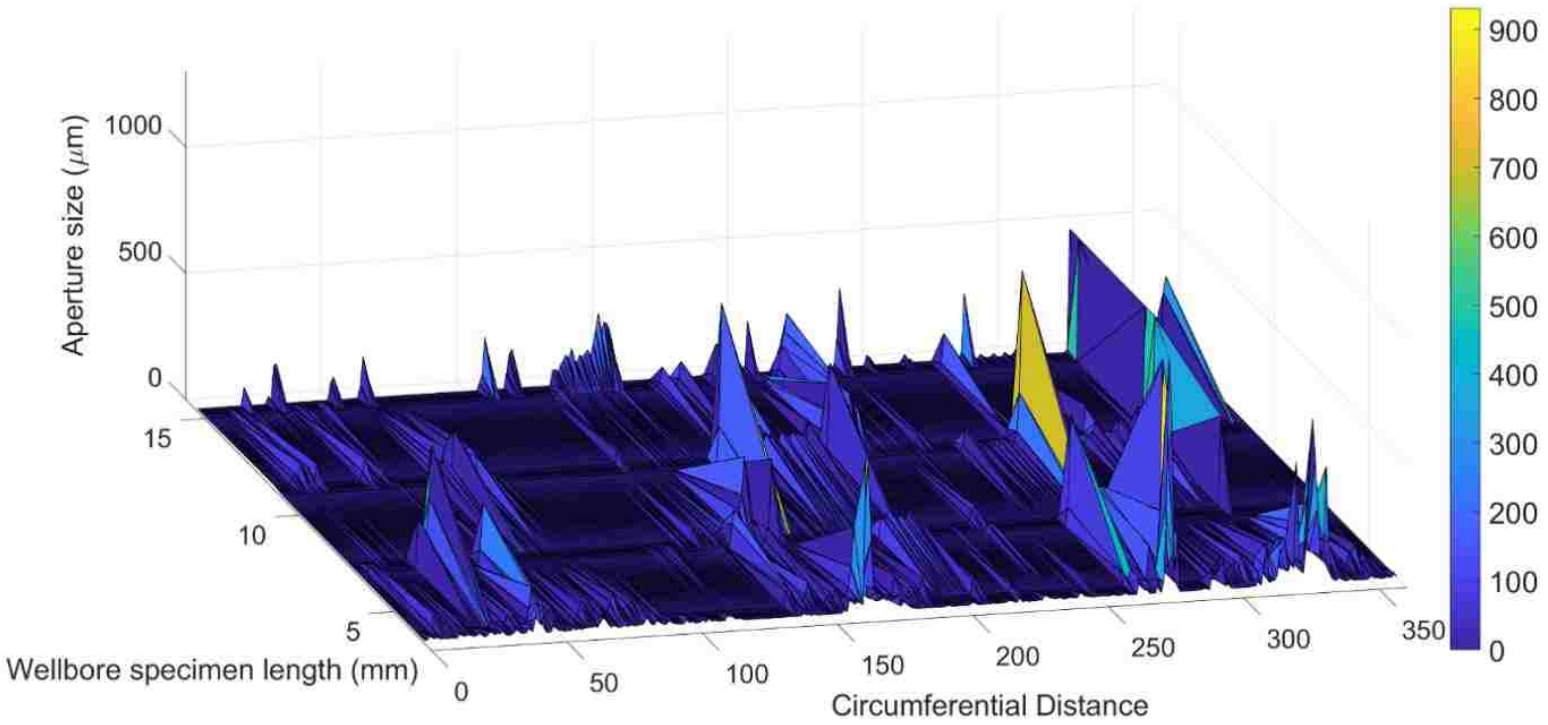

Figure 18. 3D plot of circumferential section of wellbore specimen B. 3D plot of circumferential section of wellbore specimen A. The X axis is the distance between two consecutive measurements (circumferential distance), which is the value "w" already explained, and is a measurement every degree. They Y axis is the aperture size measured in microns and the Z axis represents the position in the specimen of each circumferential section measured.

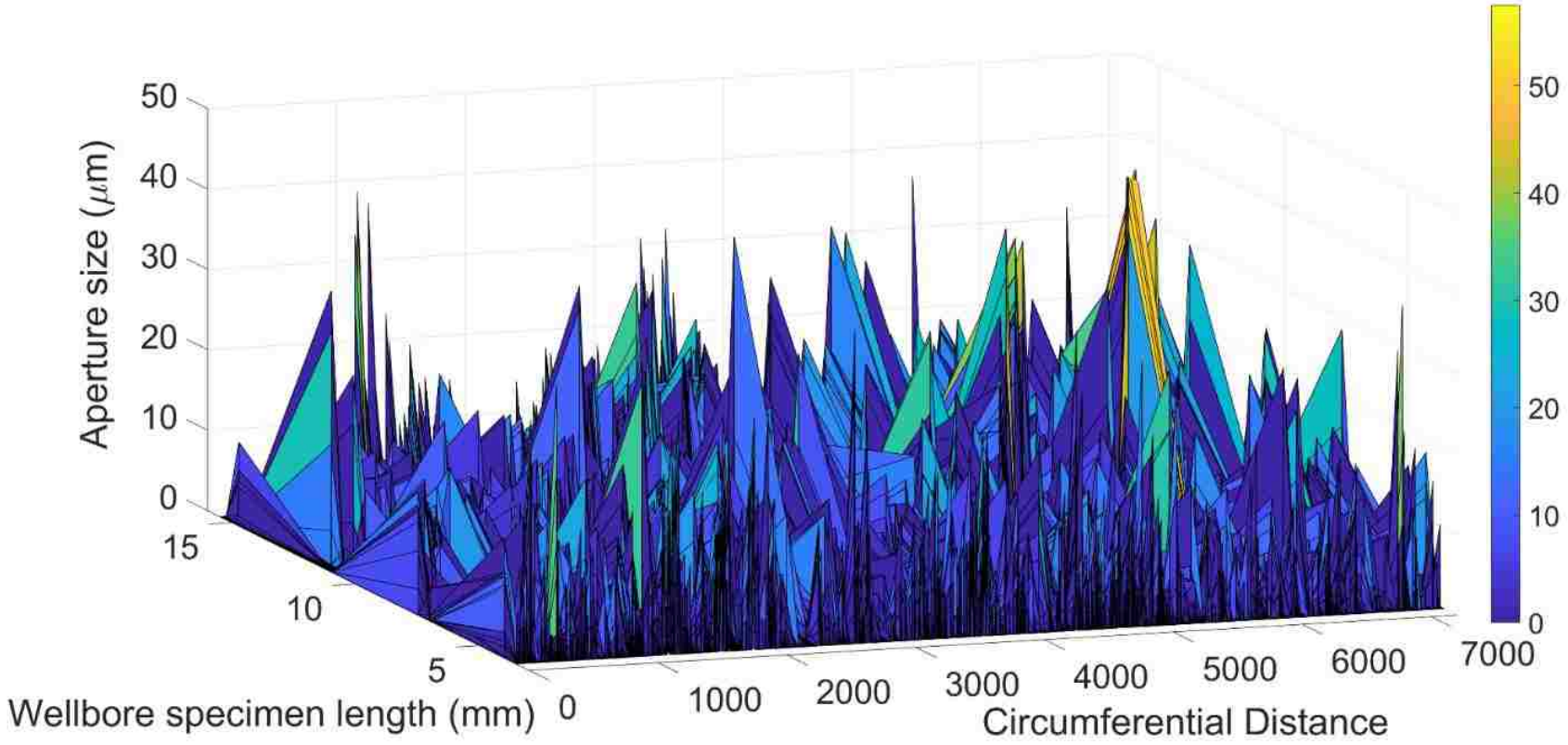

Figure 19. *3D plot of circumferential section of wellbore specimen C. 3D plot of circumferential section of wellbore specimen A.* The X axis is the distance between two consecutive measurements (circumferential distance), which is the value "w" already explained, and is a measurement every 1/20 of a degree. They Y axis is the aperture size measured in microns and the Z axis represents the position in the specimen of each circumferential section measured.

3.1 Fitting aperture data to distributions

Although the cubic law (Equation 1) is developed on the assumption of two parallel plates instead of varying aperture size, aperture sizes have been demonstrated theoretically (Brown, 1987) and experimentally (Tsang and Witherspoon, 1981) to affect fluid flow. To study how the aperture variation affects the flow and characterize this variation, aperture data for each circumferential section were fitted to various statistical distributions.

The distribution that would fit the microannuli aperture sizes is not known. We consequently looked at the distributions used to describe aperture sizes in rock fractures. Lognormal distributions have been widely reported in various rock types (Bianchi and Snow, 1969; Gale, 1987; Johns et al., 1993; Sanei et al., 2015). Other statistical distributions such as power law (Barton and Hsieh, 1989; Gale et al., 2007), normal (Asadollahi, 2009) and gamma (Gentier, 1987; Tsang and Tsang, 1987) have also been reported. Weibull was also used, since it is a distribution with characteristics similar to the lognormal. The distributions reported in the literature consist of two parameters. In addition to these, we used modifications of the distributions with additional parameters.

3.1.1 Description of the statistical distributions:

The normal distribution has two parameters: the mean value (μ) and the standard deviation (σ). The probability density function is:

$$f(x) = \frac{exp\left(-\frac{1}{2}\left(\frac{x-\mu}{\sigma}\right)^2\right)}{\sigma\sqrt{2\pi}}$$ Equation 8

Lognormal distribution has two or three parameters: the mean value (μ) and the standard deviation (σ) and the continuous location parameter (γ). γ=0 yields the two parameter (2P) lognormal. The probability density function is:

$$f(x) = \frac{exp\left(-\frac{1}{2}\left(\frac{ln(x-\mu)}{\sigma}\right)^2\right)}{(x-\gamma)\,\sigma\sqrt{2\pi}}$$ Equation 9

Weibull distribution has two or three parameters: continuous shape parameter (α>0), continuous scale parameter (β>0) and continuous location parameter γ (γ=0 yields the weibull 2P) . The probability density function is:

$$f(x) = \frac{\alpha}{\beta}\left(\frac{x-\gamma}{\beta}\right)^{\alpha-1} exp\left(-\left(\frac{x-\gamma}{\beta}\right)^{\alpha}\right)$$ *Equation 10*

The gamma distribution has two or three parameters: continuous shape parameter (α>0), continuous scale parameter (β>0) and continuous location parameter γ (γ=0 yields the gamma 2P) . The probability density function is:

$$f(x) = \frac{(x-\gamma)^{\alpha-1}}{\Gamma(\alpha)\beta^{\alpha}} \, exp\,(-(x-\gamma)/\beta) \qquad \textit{Equation 11}$$

The generalized gamma distribution has three or four parameters: continuous shape parameters (α>0 and k>0), continuous scale parameter (β>0) and continuous location parameter γ (γ=0 yields the generalized gamma 3P) . The probability density function is:

$$f(x) = \frac{k(x-\gamma)^{k\alpha-1}}{\Gamma(\alpha)\beta^{k\alpha}} \exp\left(-\left(\frac{x-\gamma}{\beta}\right)^{k}\right) \qquad \textit{Equation 12}$$

3.1.2 Distribution fitting

The Chi-square goodness-of-fit test (Luo et al., 2016) was used to evaluate the fit of the aperture data to different distributions (normal, lognormal, gamma and Weibull). Every aperture measurement is considered a discrete value (O_i) and the statistical value (χ^2) is obtained following Equation 13:

$$\chi^2 = \sum_{i=1}^{k} \frac{(O_i - E_i)^2}{E_i} \qquad \textit{Equation 13}$$

where E_i is the expected aperture value for a given distribution. The null hypothesis is that the data are consistent with a particular distribution. If the χ obtained from equation 13 is smaller than the threshold χ defined by an assumed significance value (α), we can confirm with specific significance that the data fit the distribution. Usually $\alpha = 0.05$ is used as the minimum significance value to accept the null hypothesis, but this value is

arbitrary and it depends on the sample size. We calculated up to $\alpha = 0.01$. The greater the α value is the better the data fit the particular statistical distribution

The apertures were fitted to the cited distributions in two different forms: first, all apertures measured for each wellbore specimen and second, the apertures of each circumferential section separately.

3.1.3 Results: Aperture data for each wellbore specimen

Wellbore specimen A fit the generalized gamma 4P with $\alpha = 0.02$ (Figure 20), wellbore specimen B fit the generalized gamma 4P with $\alpha = 0.1$ (Figure 21) and wellbore specimen C did not fit any distribution (Figure 22). Aperture data was fitted to all modifications of the distributions, but for clarity, we plotted two different images, one with all the distributions original distributions (i.e. lognormal) and a second one with all the modifications of the original distributions (i.e. lognormal 3P).

Wellbore specimen C did not fit any distribution. It is well-known that the likelihood a set of data will fit a distribution decreases as the number of data points increase (Diez et al., 2015). Even small differences become statistically significant when the sample becomes too large. Wellbore specimen C had 20 times more data points than wellbore specimens A and B. In addition, following the same reasoning, it was anticipated that both wellbore specimens A and B would be unable to fit many distributions as they each had already a large number of points.

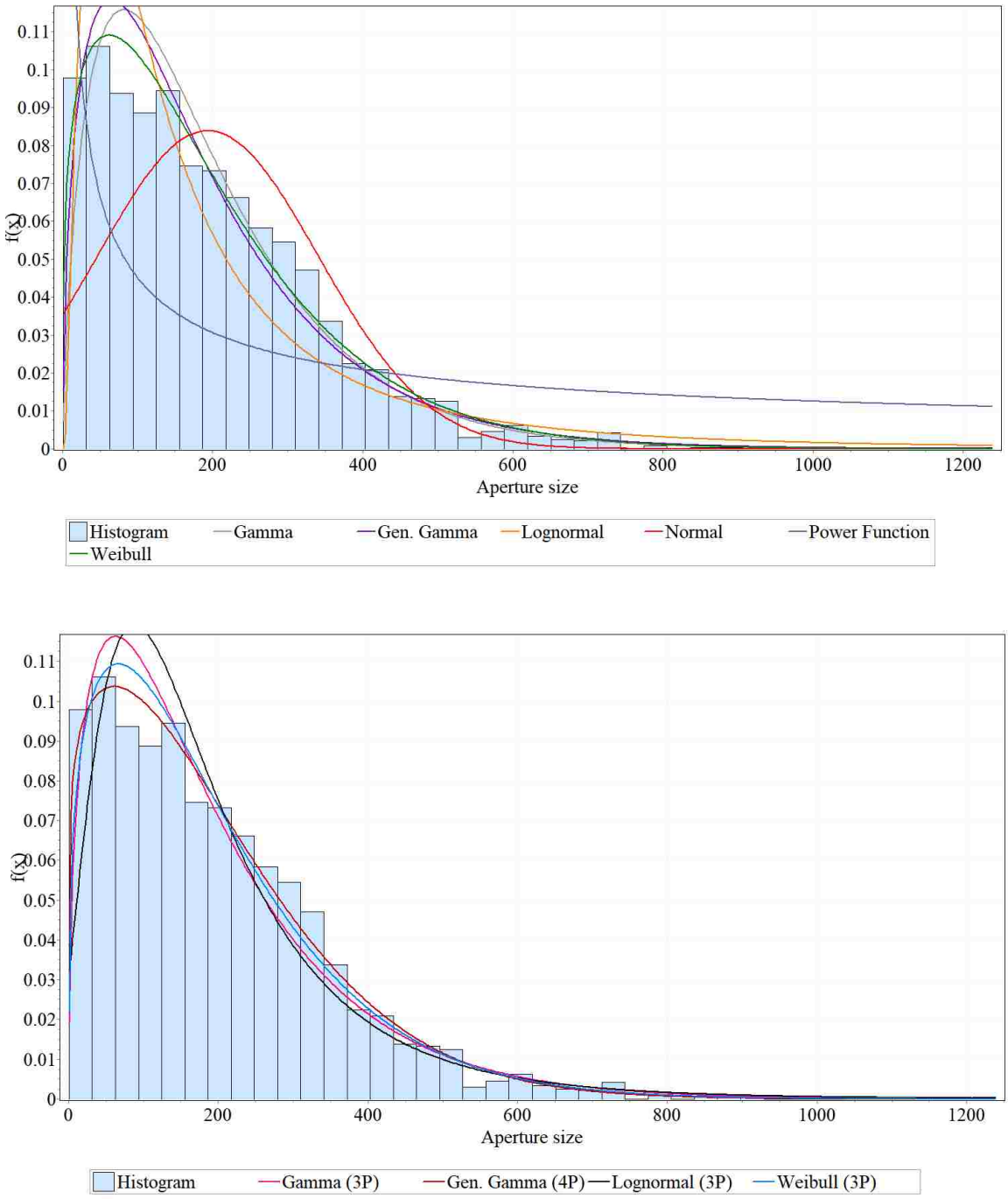

Figure 20. Aperture data from wellbore specimen A fitted to different relevant distributions. The top image has the original statistical distributions and the bottom image has the modifications.

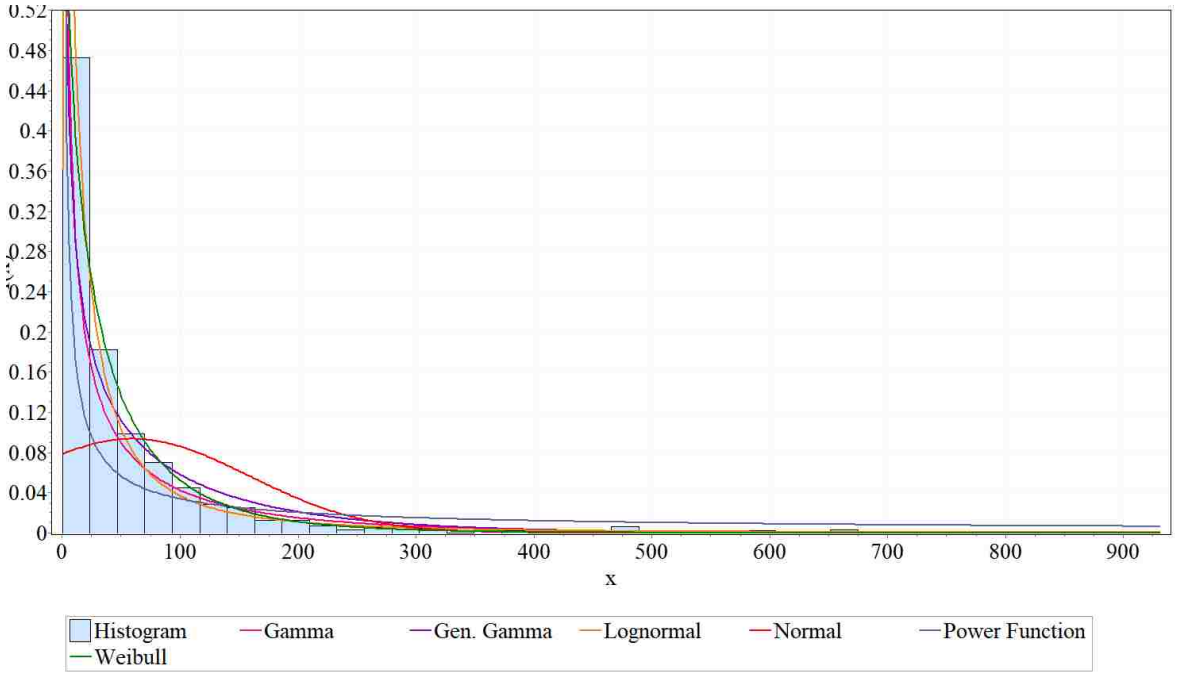

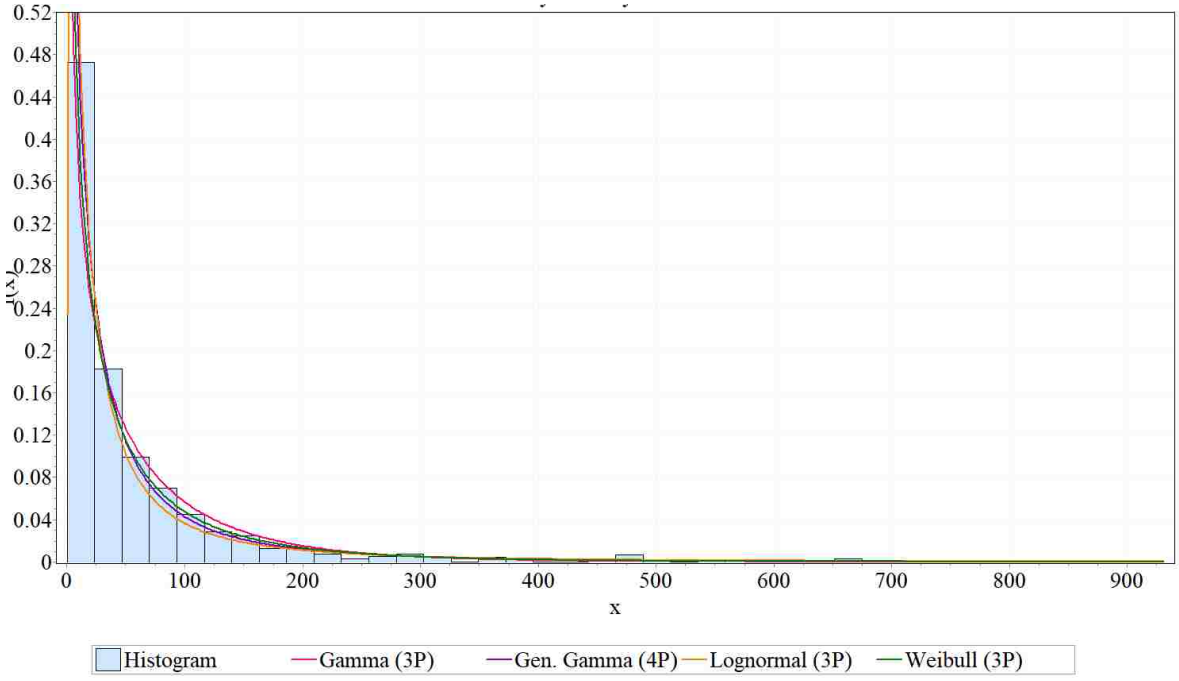

Figure 21. Aperture data from wellbore specimen B fitted to different distributions relevant distributions. The top image has the original statistical distributions and the bottom image has the modifications.

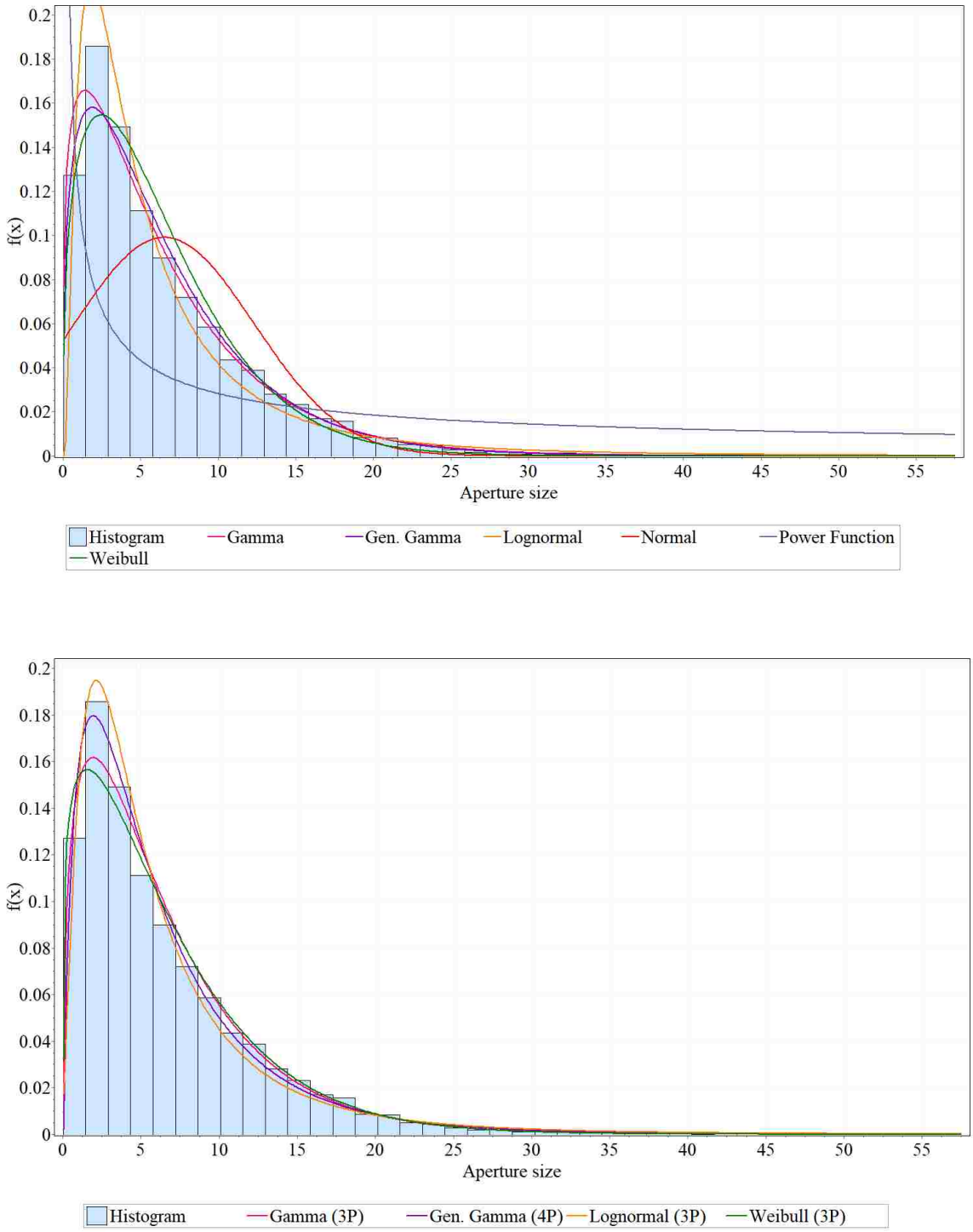

Figure 22. Aperture data from wellbore specimen C fitted to different relevant distributions. The top image has the original statistical distributions and the bottom image has the modifications.

3.1.4 Statistical Significance vs Practical significance:

The χ^2 goodness-of-fit test results are dependent on the sample size. If the number of points is too large, even a small difference would be considered statistically significant and the null hypothesis would be rejected, meaning that the data do not fit the statistical distribution proposed. While the test might conclude that there is a statistically significant difference between the statistical distribution and the experimental data, this might have no practical relevance. To show this concept, I will show two extreme cases as example. In Figure 23 we observe two different datasets. The data from the image in the top belongs to circumferential section A.2.b and the data from the bottom image belongs to the wellbore specimen C. Intuitively, it is reasonable to expect that the data from wellbore specimen C would be a good fit to the generalized gamma (4P) distribution proposed, while the data from A.2.b does not seem to fit Weibull (3P). Results from χ^2 test concluded that the data from A.2.b fits Weibull 3P with $\alpha = 0.2$, while data form wellbore specimen C does not fit. In addition, looking to the probability difference between the theoretical distribution and the experimental data support the idea that too large samples will likely not pass the χ^2 test (Figure 24). We can observe that the differences between the theoretical distributions and the experimental data are smaller in the data from wellbore specimen C, yet the test rules that generalized Gamma 4P is not a good fit.

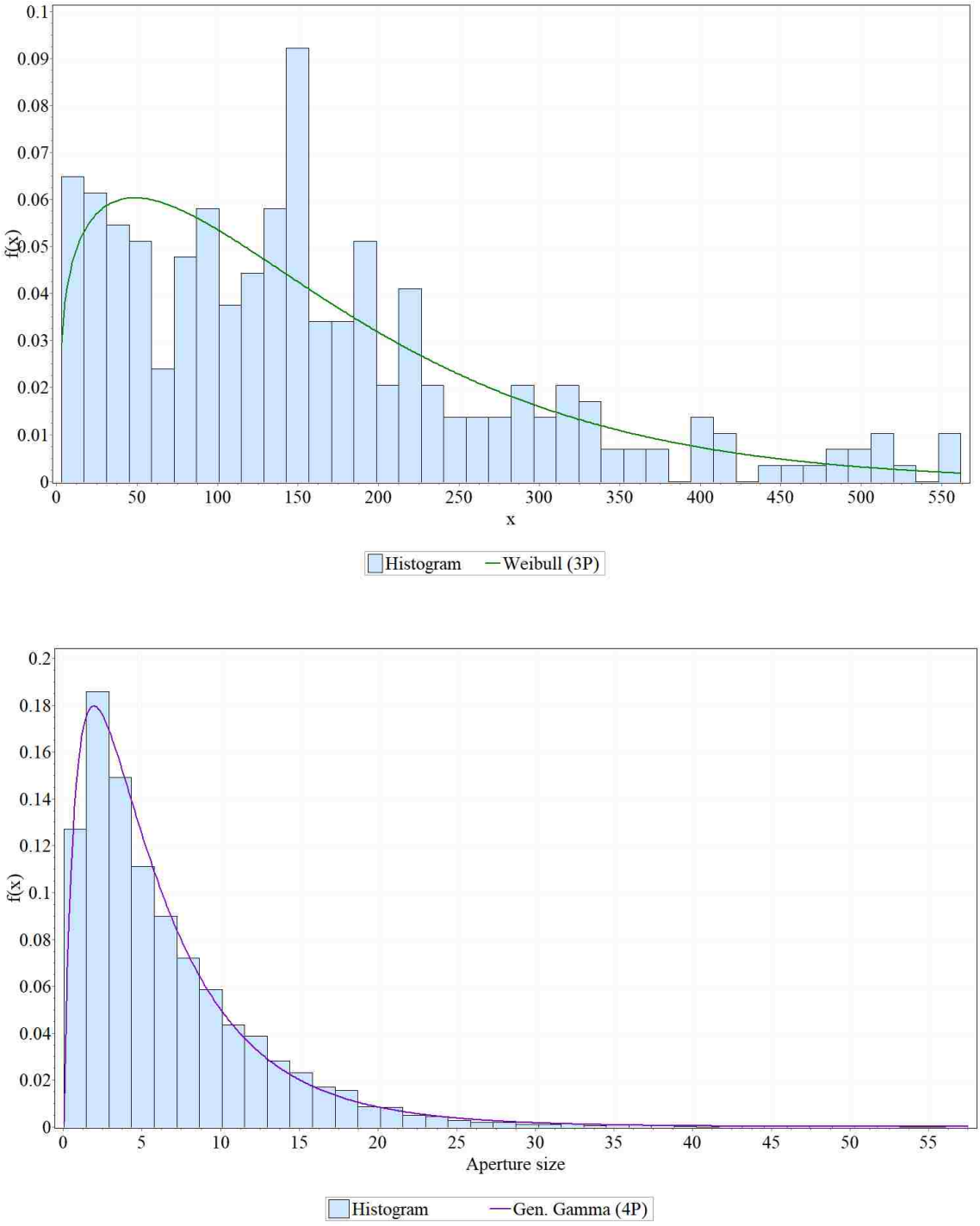

Figure 23. Comparison of two different datasets: one belongs to circumferential section A.2.b (293 points) and the other is the dataset of all the apertures measured in wellbore specimen C (10672).

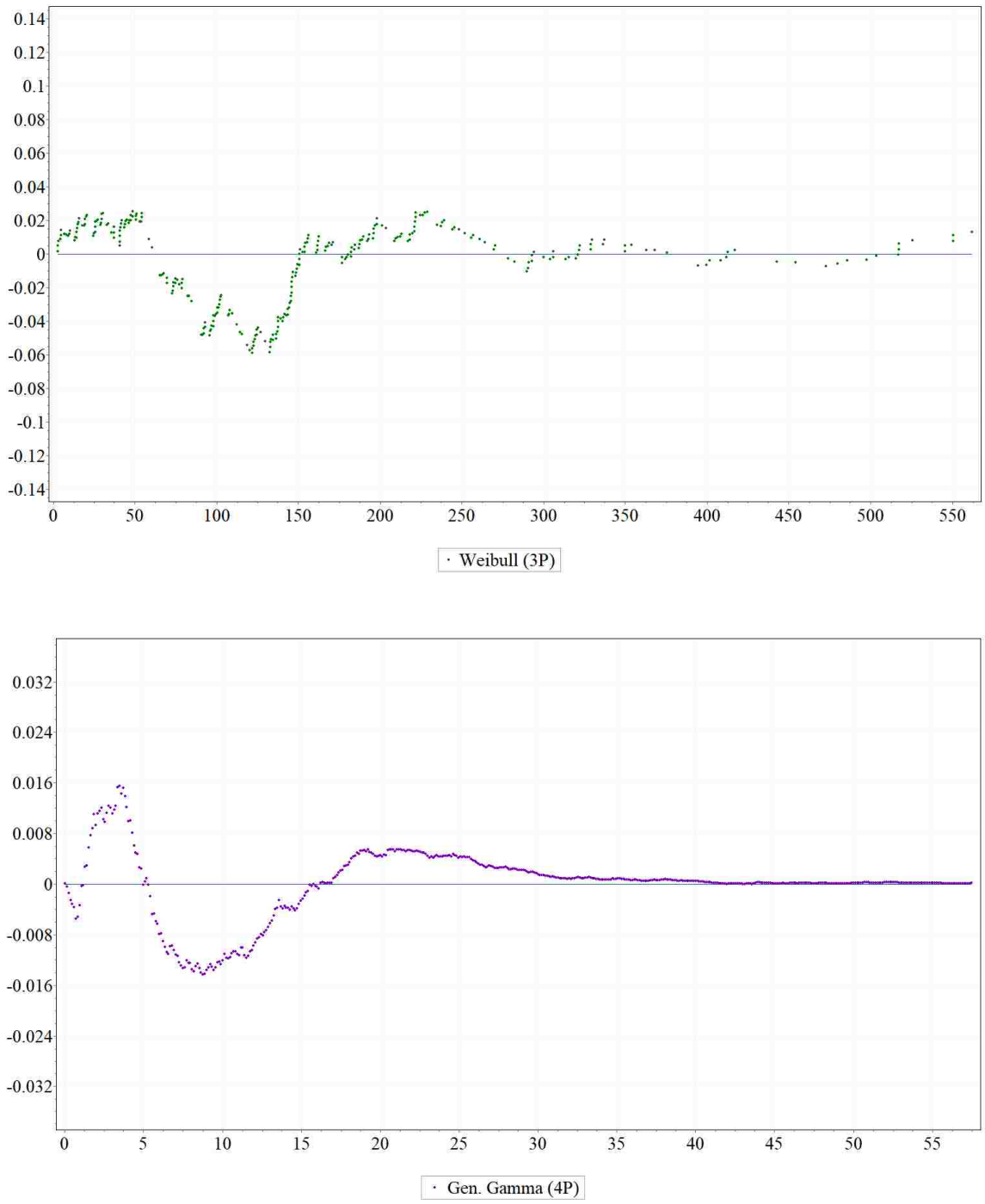

Figure 24. Example to illustrate the effect of the number of points in the dataset. Comparison of two different datasets: one belongs to circumferential section A.2.b (293 points) and the other is the dataset of all the apertures measured in wellbore specimen C

(10672). The Y axis is the probability difference between the theoretical cumulative distribution function and the experimental cumulative distribution function. Weibull (3P) fitted with α =0.2 while gen. gamma 4P did not even fit for α =0.01.

3.2 Results: Aperture data for each circumferential section

Apertures for each circumferential section were fitted to statistical distributions and the results show whether or not the sections fit the distribution and, if it does, the significance value α (Table 1). If the data did not fit the distribution, the space was left empty. Circumferential sections of wellbore specimen A did not fit the distributions consistently. Distributions such as generalized gamma 4P and lognormal 2P, fairly common in other specimens, were not present in this sample. The most frequent distribution was normal, present in five of eight sections. In wellbore specimen B, both lognormal distributions (2P and 3P) fit all sections, the Weibull distribution fit 7 of 8, and generalized gamma fit 5 of 8. In wellbore specimen C, generalized gamma 4P fit all sections, 5 of them with the highest significance value tested. Lognormal 3P fit 6 of 8, and gamma 3P and lognormal 2P fit 5 of 8. From these results, we found significant differences between the specimens and between the circumferential sections in the same specimens.

Table 1. Chi-square of wellbore specimens A, B and C. The results are presented as the significance value found to match the circumferential section. If empty, the section cannot be fitted to the distribution with a significance level of 0.01.

Wellbore Specimen	Circumferential Section	Lognormal 2P	Lognormal 3P	Normal	Power Law	Gamma	Gamma 3P	Gen. Gamma	Gen. Gamma 4P	Weibul	Weibul 3P
A	A.1.b			0.02							
	A.2.a										
	A.2.b		0.05			0.1	0.05	0.05		0.2	0.2
	A.3.a			0.2							
	A.3.b			0.1							
	A.4.a			0.01							
	A.4.b			0.1							
	A.5.a	0.1	0.1			0.02	0.05	0.1		0.1	0.1
	All A								0.02		

B	B.1.b	0.05	0.1								
	B.2.a	0.2	0.2				0.05			0.2	
	B.2.b	0.1	0.1	0.05		0.2		0.2		0.2	
	B.3.a	0.2	0.2						0.02	0.2	
	B.3.b	0.02	0.02			0.01	0.2	0.05	0.2	0.2	
	B.4.a	0.1	0.2	0.01		0.2		0.2	0.2	0.2	
	B.4.b	0.2	0.2					0.01		0.2	
	B.5.a	0.1	0.05	0.05		0.2	0.05	0.2		0.1	0.05
	All B								0.1		
C	C.1.b					0.02	0.02	0.05	0.02		0.02
	C.2.a	0.01	0.01						0.02		
	C.2.b		0.05				0.02		0.2		

	C.3.a	0.02					0.05		0.2		
	C.3.b	0.2	0.2						0.2		
	C.4.a		0.05			0.2	0.2	0.2	0.2	0.2	0.2
	C.4.b	0.01	0.2						0.05		
	C.5.a	0.05	0.2			0.2	0.2	0.2	0.2	0.2	0.2
	All C										

From Table 1, we observed that even though all the sections of specimens B and C fit a distribution, all the data as a whole do not fit these same distributions, as is the case in samples B and C. The explanation for this result is although every circumferential section fir the same statistical distribution, each distribution has its own parameters.

To further investigate the variability of the different circumferential sections in a wellbore specimen, the two-sample Kolmogorov-Smirnoff test was performed between sections of the same specimen (Massey, 1951). This test compares the empirical cumulative distribution of the apertures in two different sections and determines whether both aperture data belong to the same statistical distribution. It does not provide information about which distribution the aperture data derive from nor define the parameters of the statistical distribution.

The results showed that 5 of 25 cross tests were false (Table 2), which means that there are five combinations of sections obtained from the same distribution, being A.4.a and A.4.b the only consecutives separated by a circumferential section thickness (35mm). For specimen B, we found seven combinations of surfaces from the same distribution (Table 3); the only consecutives were B.4.a and B.4.b, separated by 35mm. For specimen C, the results showed that six combinations of sections were from the same distribution (Table 4). The consecutives were C.4.b and C.5.a (separated by just 17.5 mm); C.2.a and C.3.a were separated by the same distance (35 mm) as the consecutive surfaces in samples A and B. The original hypothesis was that consecutive circumferential sections had higher probability of being derived from the same statistical distribution since they are physically closer, but we found that, in most cases, they are not related. We found that no surface separated just by the blade thickness (3.5mm) derive from the same

distribution. These results support the idea of significant aperture variability along the specimens.

Table 2. Kolmogorov-Smirnoff test between surfaces of wellbore specimen A. False means they derive from the same distribution, whereas true means they do not.

	A.1.b	A.2.a	A.2.b	A.3.a	A.3.b	A.4.a	A.4.b	A.5.a
A.1.b	FALSE	TRUE	TRUE	TRUE	TRUE	TRUE	TRUE	TRUE
A.2.a	TRUE	FALSE	TRUE	TRUE	TRUE	TRUE	TRUE	TRUE
A.2.b	TRUE	TRUE	FALSE	TRUE	FALSE	TRUE	TRUE	FALSE
A.3.a	TRUE	TRUE	TRUE	FALSE	TRUE	FALSE	TRUE	TRUE
A.3.b	TRUE	TRUE	FALSE	TRUE	FALSE	TRUE	TRUE	FALSE
A.4.a	TRUE	TRUE	TRUE	FALSE	TRUE	FALSE	FALSE	TRUE
A.4.b	TRUE	TRUE	TRUE	TRUE	TRUE	FALSE	FALSE	TRUE
A.5.a	TRUE	TRUE	FALSE	TRUE	FALSE	TRUE	TRUE	FALSE

Table 3. Kolmogorov-Smirnoff test between surfaces of wellbore specimen B. False means they derive from the same distribution, and true means they do not.

	B.1.b	B.2.a	B.2.b	B.3.a	B.3.b	B.4.a	B.4.b	B.5.a
B.1.b	FALSE	TRUE	TRUE	FALSE	TRUE	TRUE	FALSE	TRUE
B.2.a	TRUE	FALSE	TRUE	TRUE	TRUE	TRUE	TRUE	TRUE
B.2.b	TRUE	TRUE	FALSE	TRUE	FALSE	TRUE	TRUE	FALSE
B.3.a	FALSE	TRUE	TRUE	FALSE	TRUE	TRUE	FALSE	TRUE
B.3.b	TRUE	TRUE	FALSE	TRUE	FALSE	TRUE	TRUE	FALSE
B.4.a	TRUE	TRUE	TRUE	TRUE	TRUE	FALSE	FALSE	TRUE
B.4.b	FALSE	TRUE	TRUE	FALSE	TRUE	FALSE	FALSE	TRUE
B.5.a	TRUE	TRUE	FALSE	TRUE	FALSE	TRUE	TRUE	FALSE

Table 4. Kolmogorov-Smirnoff test between surfaces of wellbore specimen C. False means they derive from the same distribution; true means they do not.

	C.1.b	C.2.a	C.2.b	C.3.a	C.3.b	C.4.a	C.4.b	C.5.a
C.1.b	FALSE	TRUE	TRUE	TRUE	TRUE	TRUE	TRUE	TRUE
C.2.a	TRUE	FALSE	TRUE	FALSE	TRUE	TRUE	FALSE	FALSE
C.2.b	TRUE	TRUE	FALSE	TRUE	TRUE	TRUE	TRUE	TRUE
C.3.a	TRUE	FALSE	TRUE	FALSE	TRUE	TRUE	FALSE	FALSE

C.3.b	TRUE	TRUE	TRUE	TRUE	FALSE	TRUE	TRUE	TRUE
C.4.a	TRUE	TRUE	TRUE	TRUE	TRUE	FALSE	TRUE	TRUE
C.4.b	TRUE	FALSE	TRUE	FALSE	TRUE	TRUE	FALSE	FALSE
C.5.a	TRUE	FALSE	TRUE	FALSE	TRUE	TRUE	FALSE	FALSE

3.3 Microannulus aperture uniformity

The microannulus is often characterized by its hydraulic aperture from interpreting flow data, which assumes the aperture is constant along and around the wellbore. To check aperture uniformity, we performed two studies with the wellbore specimen aperture data for aperture variability of the microannuli. One study focused on aperture variability from the top to the bottom of samples, and the other tested the correlation between apertures in circumferential sections.

3.3.1 Vertical aperture variability

Tortuosity and contact affect the fluid flow through fractures, altering the interpretation of fracture size using the cubic law (Equation 1). Since only 8 discrete circumferential sections were studied for each specimen, there was incomplete knowledge of aperture variance between the analyzed sections, which precluded obtaining a complete and precise estimation of the tortuosity or the change of the contact areas within the microannulus.

Despite the fact that wellbore specimens are cylindrical, the apertures measured could be represented “unfolded” in a plane (Figure 17),(Figure 18),(Figure 19). This interpretation aids understanding of the subsequent experiment; if a specimen has no tortuosity, the flow follows a straight top-to-bottom path, and the distance traveled by the gas equals the specimen length.

We selected all the aperture measurements in the top circumferential section, one at a time, and moved to the bottom circumferential section, testing whether it formed a continuous flow path along the axis of the wellbore or if there was contact. For instance, starting from a measurement that is not 0 in the top circumferential section, we move to the second circumferential section at the very same location and check what is the aperture size measurement. If the aperture is 0, it means there is contact between the steel and the cement, hence there is no continuous flow path. If the aperture is not equal to zero, we move to the next circumferential section. This was repeated for every split “w”, which means that in wellbore specimens A and B we study 360 “flow paths” and in wellbore specimen C, 7200. Following the same approach, we looked for continuous contact paths along the specimens. For that, we looked for constant zero values along the specimen vertical axis instead of nonzero as we did for continuous flow paths. These processes were done using specimens A, B and C; the results are shown in Table 5:

Table 5. Number of continuous vertical flow paths and continuous vertical contact along the sample length. For specimens A and B, values are for a total of 360 measurements per section. In the case of sample C, 7200 total measurements were made.

	Continuous paths	Continuous paths %	Continuous contact	Continuous contact %
Wellbore Specimen A	94	26.11	0	0
Wellbore Specimen B	0	0	16	4.44
Wellbore Specimen C	1	0.01	1329	18.46

It was anticipated that vertical continuous contact would increase as we proceeded from a specimen with low contact percentage (A) to a sample in which most circumferential sections have more than 80% contact (C) (Table 8). The same reasoning applied to a decrease in the number of continuous paths.

If the samples are understood as a flow system with as many potential flow paths as aperture measurements performed (360 for A and B, 7200 for C), sample A had 26.11% continuous paths. In other words, 73.89% of the flow paths in this sample, in at least one point along the specimen, are closed; consequently fluid moving through microannulus would have to deviate from a straight path. In addition, what we define here as a continuous path might not actually be the case, since we do not know how the apertures change between the surfaces analyzed. This consideration indicates that the percentages shown as continuous paths are in fact the largest possible number of continuous paths in

the specimens. All these deviations increase the actual distance that the flow travels and are deviations from the assumed geometry (straight flow path).

Another component of the tortuosity is the change in aperture size in the direction of the flow, since any change in aperture deviates the flow from a straight line. Every two consecutive measurements had a different aperture. Because of that, we already assume that this component of the tortuosity is a constant throughout the wellbore specimens.

This component, in addition to the continuity of the flow paths, will deviate the flow measurement interpretations from the cubic law. Greater deviations were anticipated in samples B and C, as they had virtually no straight flow paths and all the gas must travel a greater distance than the sample length. Because we had only discrete measurements, we were unable to quantify the degree to which this affects the interpretation of the cubic law.

3.3.2 Horizontal correlation in circumferential sections

Correlation tests were performed in the measured apertures of each circumferential section to question the assumption of uniformity (Diez et al., 2015; Neville and Kennedy, 1964) in the apertures used to derive the local cubic law (Equation 1). This test quantifies the linear correlation of the apertures of the same circumferential section. If the apertures are uniform around the steel casing, the correlation coefficient should be 1. The smaller the correlation value, the less linearly correlated the apertures are. In addition, the results of the correlation test offer an approximation of the variability of the aperture magnitude and range. The equation of the correlation is:

$$r = \frac{n\sum xy - \sum x \sum y}{\sqrt{(n\sum x^2 - (\sum x)^2)(\sum y^2 - (\sum y)^2)}} \qquad \textit{Equation 14}$$

Where r is the correlation coefficient (between -1 and 1), n is the number of points, and x and y are the sets of data that we are correlating, which are aperture measurements of the same circumferential section but with certain lag. The lag is the distance between the measurements that we are testing for. We started studying the correlation between consecutive measurements, and we called that lag 1. Then we studied lag 2, lag 5 and lag 10. For example, when talking about lag 1, we compared the first with the second measurement, then the second with the third and so on. For lag 2, we studied first with third, second with forth… For lag 5 it was first with sixth, second with seventh… and for lag 10 it was first with eleventh, second with twelfth and so on. Theoretically, the correlation between aperture measurements should decrease as we increase the lag.

For specimens A and B, lag 1 was 510 μm, which is the horizontal distance between measurements; for sample C, lag 1 was 25 μm. Wellbore specimen A showed strong correlation values in all sections (correlation coefficient >0.8); surface A.2.a alone had a correlation length of 1020 μm (lag 2). In specimens B and C, no circumferential section showed correlation with lag 1. These results indicate that there is a linear relation between consecutive measurements only in wellbore specimen A. In wellbore specimens B and C, the low r found with all the coefficient indicate that the apertures are far from being uniform.

3.4 Convergence studies

Two convergence studies were performed on the wellbore specimens. The first evaluated how many circumferential sections must be analyzed to predict the permeability characteristics of a specimen. The second was to obtain a characteristic aperture length of the microannulus, which can be achieved by changing the 'w', and estimating the error produced when too large a 'w' is used. The characteristic aperture length is the typical width that the apertures of the microannulus have. In other words, the width of the apertures in between contact points.

The characteristics that we refer in this study are related to the apertures measured and the interpreted hydraulic apertures from such measurements. Five parameters were used to analyze the sections: mean aperture, mean aperture including the zero values of the apertures, the cubic law (Equation 1), the geometric mean and the modification of the cubic law made by Renshaw, 1995:

$$h = \bar{x} * \left(1 + \frac{\sigma^2}{\bar{x}}\right)^{\left(\frac{-1}{2}\right)} \qquad \textit{Equation 15}$$

Where $\overline{x}$ is the arithmetic mean of the mechanical aperture and σ^2 is the variance of the mechanical aperture. We applied this equation because it is widely used and it was developed under the assumption that apertures follow a lognormal distribution, which seems reasonable from what we observed in our experimental data.

Both means are presented here to show a meaningful conceptual difference; that is, to define whether we refer to the microannulus alone or to the cement-casing interface.

When referring to the microannulus only, the zero values should not be included. By definition, the microannulus is the space between the cement and the steel casing; if there is no aperture, there is no microannulus. If we discuss the entire cross-section, the zero values should be included. Mean with zero values provide a direct comparison between the interpreted hydraulic aperture and an uniform mean aperture around the circumferential section, as the parallel plate assumption.

3.4.1 Number of circumferential sections

The purpose of this convergence study was to determine how many sections should be analyzed per wellbore specimen to achieve a satisfactory approximation of aperture characteristics; that means that we find an approximation to the solution obtained with 7200 aperture measurements with less data points and the difference between the approximation and the 7200-obtained value has a small error that could be tolerated. We selected circumferential sections that were as equally spaced as possible. For example, when just one surface was used, it was located at the middle of the specimen and when two surfaces were selected, they were located at 1/3 and 2/3 of the sample length.

The results show the weighted average of the parameters used (Table 6), with weighting done using the contributive length of each section. This approach was used because the circumferential sections were not equally spaced, as some were spaced only by the thickness of the blade used to section them and others by more than 30 mm. There was no significant difference between this approach and the just averaging the circumferential section values, but we used it as we considered it to represent better the geometry of the

problem. In general, we observed few changes relative to the number of surfaces. Although the values obtained differed, all were in a close range of values (Table 6).

Table 6. Convergence study of the number of circumferential sections needed to represent and characterize the microannuli of a specimen

Wellbore Specimen	Property	1 Surface (µm)	2 Surfaces (µm)	3 Surfaces (µm)	4 Surfaces (µm)	8 Surfaces (µm)
A	Mechanical Mean	200.50	168.43	164.42	179.91	188.12
	Mean with 0's	166.53	134.92	134.74	150.60	156.83
	LCL	269.49	232.70	232.05	255.55	268.14
	Renshaw	240.46	207.85	200.83	221.66	232.31
	Geometric Mean	141.89	117.47	123.80	129.67	133.65
B	Mechanical Mean	31.24	53.46	67.18	56.79	55.66
	Mean with 0's	8.16	12.27	25.02	17.00	16.77
	LCL	74.41	84.44	136.74	103.37	111.31
	Renshaw	71.81	91.47	128.70	104.43	107.83
	Geometric Mean	9.24	22.94	22.69	19.97	18.50
C	Mechanical Mean	5.32	7.85	6.77	6.82	6.41

	Mean with 0's	0.59	1.19	1.21	1.36	1.18
	LCL	12.53	18.84	16.71	18.18	17.11
	Renshaw	7.26	10.17	8.66	8.90	8.47
	Geometric Mean	3.63	5.71	4.77	4.79	4.44

3.4.2 3.2 Different ‘w’ in wellbore specimen C

The aperture around the sample must be accurately represented to later interpret a hydraulic aperture. The smaller the circumferential incremental distance (“w”) used, the larger the number of areas measured, leading to a more accurate representation of the aperture (Figure 11), but more computationally expensive. To depict the apertures of the circumferential sections analyzed as accurate as possible while computationally efficient , we performed a convergence study to determine the ‘w’ that yielded the most acceptable results (in terms of less error compared to the results obtained from the smaller “w”, which conceptually are the most accurate result) with the smallest number of measurements (see Table 7).

Table 7. Convergence study of wellbore specimen C. Several widths were tested to find a characteristic length of the apertures. The change in percentage is calculated for LCL, mean mechanical aperture and contact percentage. The changes are calculated between consecutive smaller widths. For instance, the change (in percentage) when moving from using 510 µm as "w" to 255.00 µm in the hydraulic aperture interpreted from the LCL in circumferential section C.1.b is an increase of 16.79%.

Circumferential Section	"w" value (µm)	LCL (µm)	Mean Mechanical aperture (µm)	Contact	Change % LCL	Change % Mean mech. Aperture	Change % contact
C.1.b	25.50	7.11	7.22	0.76	10.25	27.75	9.36
	51	6.45	5.65	0.70	11.69	34.50	17.46
	102	5.77	4.20	0.60	21.24	47.12	47.22
	255	4.76	2.85	0.40	16.79	27.27	67.24
	510	4.08	2.24	0.24			
C.2.a	25.50	5.22	5.41	0.81	15.57	33.67	8.61
	51	4.52	4.05	0.75	17.57	41.98	16.75
	102	3.84	2.85	0.64	28.34	58.60	49.71
	255	2.99	1.80	0.43	12.10	30.27	68.68

	510	2.67	1.38	0.25			
C.2.b	25.50	6.29	5.56	0.78	8.24	31.68	9.73
	51	5.82	4.22	0.71	15.79	37.51	17.89
	102	5.02	3.07	0.60	29.60	53.93	54.73
	255	3.88	1.99	0.39	16.79	28.47	80.13
	510	3.32	1.55	0.22			
C.3.a	25.5	7.50	6.74	0.78	6.23	26.37	7.81
	51	7.06	5.33	0.73	6.66	32.65	13.91
	102	6.62	4.02	0.64	15.93	49.23	38.55
	255	5.71	2.69	0.46	37.20	34.54	67.68
	510	4.16	2.00	0.28			
C.3.b	25.5	4.42	5.32	0.89	11.57	41.72	5.53
	51	3.96	3.75	0.84	12.83	45.87	9.42
	102	3.51	2.57	0.77	18.60	75.30	29.14
	255	2.96	1.47	0.60	12.96	42.96	41.12
	510	2.62	1.03	0.42			

C.4.a	25.5	6.01	8.30	0.87	10.00	25.25	3.82
	51	5.46	6.62	0.84	9.21	36.13	7.34
	102	5.00	4.87	0.78	13.96	55.77	18.24
	255	4.39	3.12	0.66	7.75	39.92	25.53
	510	4.07	2.23	0.53			
C.4.b	25.5	5.74	5.43	0.72	8.33	24.23	10.39
	51	5.29	4.37	0.65	10.15	30.62	19.48
	102	4.81	3.35	0.55	13.58	39.53	48.94
	255	4.23	2.40	0.37	7.88	23.25	67.09
	510	3.92	1.95	0.22			
C.5.a	25.5	6.56	10.72	0.90	9.73	18.93	2.23
	51	5.98	9.02	0.88	7.99	24.60	3.58
	102	5.54	7.24	0.85	14.20	44.02	8.66
	255	4.85	5.02	0.78	7.50	33.33	10.43
	510	4.51	3.77	0.71			

The conclusions are presented in the three categories shown in Table 7:

- Cubic law:
    - The interpreted hydraulic aperture increases as the number of measurements increase because it is dependent on the cube of the aperture. The more accurately the aperture peaks are characterized and isolated, the higher the conductivity values that will be found. We found changes of orders of magnitude between the calculated hydraulic apertures with widths of 510 and 25.5 μm.
- Mean mechanical aperture
    - The mean mechanical aperture increases as the number of measurements increases. If the 'w' adopted to measure the apertures is not sufficiently small, there will be points of contact averaged with the true aperture. This misrepresentation of the apertures would lead to underestimation of the mean mechanical aperture.
- Contact percentage
    - The contact percentage increases as we increasingly use a smaller "w".
    - Contact percentage is dependent on the contact distribution and the aperture concentration around the steel casing.

3.5 Hydraulic aperture and flow measurement comparison

The aperture obtained from the image analysis was compared to the interpreted hydraulic aperture obtained from the flow measurements. Since the image analysis provides thousands of discrete measurements of the aperture rather than the single value that the flow test provides, data interpretation was required. The parameters interpreted from the image analysis were the mechanical mean (mean without the 0 values), the mechanical mean with zeros, the local cubic law for each microannulus measurement, the geometric mean and Renshaw's modification of the local cubic law (Renshaw, 1995) . The local cubic law modification developed by (Zimmerman and Bodvarsson, 1996) was tested, but was found to yield negative values, as the variance of some surfaces is greater than the mean (Equation 17):

$$h^3 = \bar{x}^3\left(1 - \frac{1.5\sigma^2}{\bar{x}^2}\right) \qquad \textit{Equation 16}$$

The eight values per sample were averaged, considering the proportion of the sample length they contribute, as explained in the section "different circumferential sections". Results are shown in Table 8. The discussion of the results is organized by wellbore specimen and are presented in bullet points:

Table 8. Wellbore specimens A, B and C with all circumferential sections, showing measured and interpreted characteristics. The interpreted vertical values obtained after image analysis processing can be compared with the interpreted hydraulic aperture obtained from the flow test.

Wellbore Specimen	Circumferential Section	Contact %	Mechanical mean (µm)	Mean with 0's	LCL (µm) (Equation 1)	Renshaw (µm) (Equation 16)	Geometric Mean (µm)	Measured (µm)
A	A.1.b	0.01	256.8	253.3	355.6	310.9	182.9	
	A.2.a	0.16	227.9	190.6	328.9	297.6	135.7	
	A.2.b	0.19	162.8	132.5	225.1	205.0	110.7	
	A.3.a	0.17	200.5	166.5	257.8	240.5	141.9	
	A.3.b	0.22	153.3	119.3	201.2	186.3	116.0	
	A.4.a	0.21	195.2	153.5	245.0	235.2	140.5	
	A.4.b	0.19	175.7	143.0	244.1	221.0	117.5	
	A.5.a	0.18	159.8	131.8	225.9	198.6	123.6	
	Weighted average		188.1	156.8	256.5	232.3	133.7	175.0

B	B.1.b	0.33	51.0	34.4	190.4	133.6	12.0	
	B.2.a	0.51	62.6	30.6	134.0	101.5	44.3	
	B.2.b	0.79	75.6	15.8	93.9	116.4	39.8	
	B.3.a	0.74	31.2	8.2	71.2	71.8	9.2	
	B.3.b	0.69	81.6	24.9	146.1	148.1	34.3	
	B.4.a	0.76	44.9	11.0	77.9	82.3	17.4	
	B.4.b	0.81	51.3	9.8	90.5	108.8	12.6	
	B.5.a	0.71	79.3	23.1	97.5	115.6	38.1	
	Weighted average		55.7	16.8	106.5	107.8	18.5	50.0
C	C.1.b	0.76	7.2	1.7	7.1	9.4	5.0	
	C.2.a	0.81	5.4	1.3	5.2	7.2	3.8	
	C.2.b	0.78	6.7	1.5	7.5	9.5	4.5	
	C.3.a	0.89	5.3	0.6	4.4	7.3	3.6	
	C.3.b	0.87	8.3	1.1	6.0	10.2	6.1	
	C.4.a	0.90	10.8	1.1	6.5	12.4	9.1	

	C.4.b	0.78	5.6	1.2	6.3	7.8	3.7	
	C.5.a	0.72	5.4	1.5	5.7	7.2	3.7	
	Weighted average		6.4	1.2	6.0	8.5	4.4	32.0

The mean mechanical aperture for wellbore specimen A was the value closest to the interpreted hydraulic aperture (only 7.5% higher). The mean with zeros underestimated the hydraulic aperture by 10.4%. LCL overestimated the aperture by 46.5%, and the geometric mean underestimated it by 33.6%. For wellbore specimen B, the mean mechanical aperture is again the closest value found compared to the hydraulic aperture interpreted from the flow test. The mechanical mean including the zeros was far from the flow test (16.8 vs. 50 μm), because the percent of contact in this sample was higher than in specimen A. LCL yielded a hydraulic aperture more than twice as large as that interpreted from the flow measurement. Geometric mean underestimated the aperture (18.5 vs. 50 μm). In the case of wellbore specimen C, we found a radial crack after testing that might have affected the hydraulic aperture measured in the flow test. For this reason, results might not be applicable.

3.6 Capillary entry pressure

One of the problems reported for CO_2 sequestration is gas migration (Barlet-Gouedard et al., 2006). Gas injected into depleted oil and gas reservoirs finds its way to the surface or pollutes groundwater (Jackson et al., 2013; Osborn et al., 2011). A potential pathway for CO_2 migration is via wellbore microannuli. Brine is frequently used in oil and gas extraction, and it is common to find it surrounding the wellbore, which facilitates filling of the microannuli with brine.

To displace the brine, gas would have to flow through the microannuli, the necessary pressure is directly related to aperture size. We used the measured apertures to estimate the capillary entry pressure (CEP) needed for gas to flow. Each measurement was considered as an individual aperture, and a range capillary entry pressures was obtained for every circumferential section of each sample. These results were compared to the capillary entry pressure estimated from the flow test. The capillary entry pressure equation is:

$$P_c = \frac{2 * \lambda * \cos\theta}{h} \qquad \text{Equation 17}$$

Where P_c is the capillary entry pressure in Pascals, λ is the interfacial tension between CO_2 and water, θ is the contact angle of the brine and gas with the cement, obtained from (Chiquet et al., 2007), and h is a discrete aperture measurement (Blunt, 2017).

3.6.1 Wellbore Specimen A

The interpretation of the flowmeter test of wellbore specimen A yielded a hydraulic aperture of 175 µm. Using this aperture, we calculated the CEP of 0.26 MPa to displace brine using (Equation 17). This interpretation of the CEP is the only possible when the only data available is from the flow test. To show its limitations, we used the measured aperture sizes and we plot the cumulative distribution function of the CEP range for each circumferential section (Figure 25). The interpreted CEP would be sufficient to displace brine with gas through 35% to 65% of the MA of the different circumferential sections.

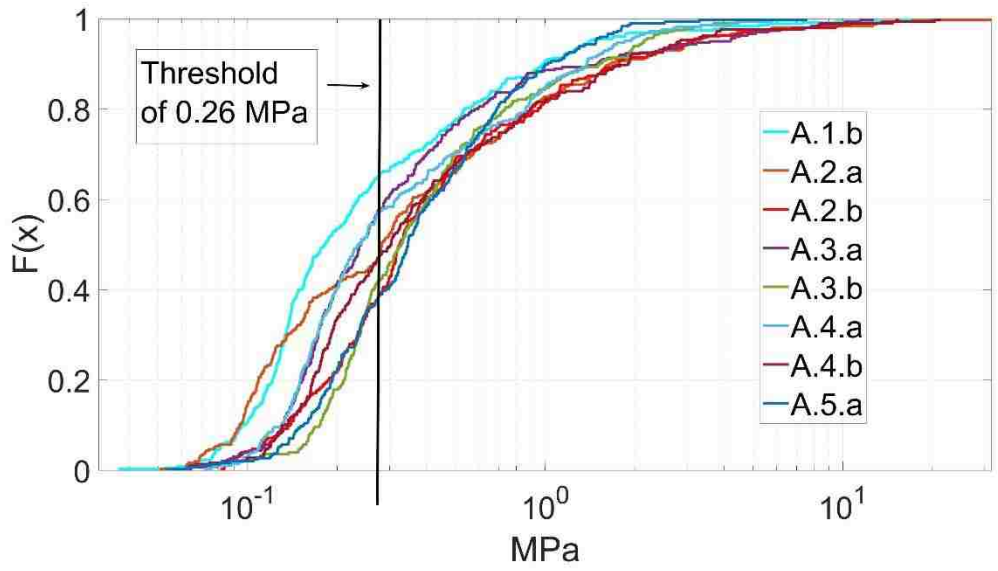

Figure 25. Capillary entry pressure of the wellbore microannuli in all circumferential sections of wellbore specimen A. There is uniformity in the shape of the cumulative curve, although there is a wide range among the surfaces.

3.6.2 Wellbore specimen B

Interpretation of the flowmeter test for wellbore specimen B yielded a hydraulic aperture of 50 µm and a permeability of $4.42 * 10^{-13}\ m^2$. Using the hydraulic aperture, we obtained the capillary entry pressure needed to displace the brine (Equation 17), which was 0.92 MPa. Since we measured actual aperture size, we were able to plot the whole capillary pressure range (Figure 26); we determined that the interpreted capillary entry pressure would be sufficient to displace brine with gas through 15% to 55% of the apertures of the microannuli. The CEP estimated from the flow test is a considerable underestimation of

the pressure necessary to move the gas through the small apertures. We found a wide range of CEP among the surfaces.

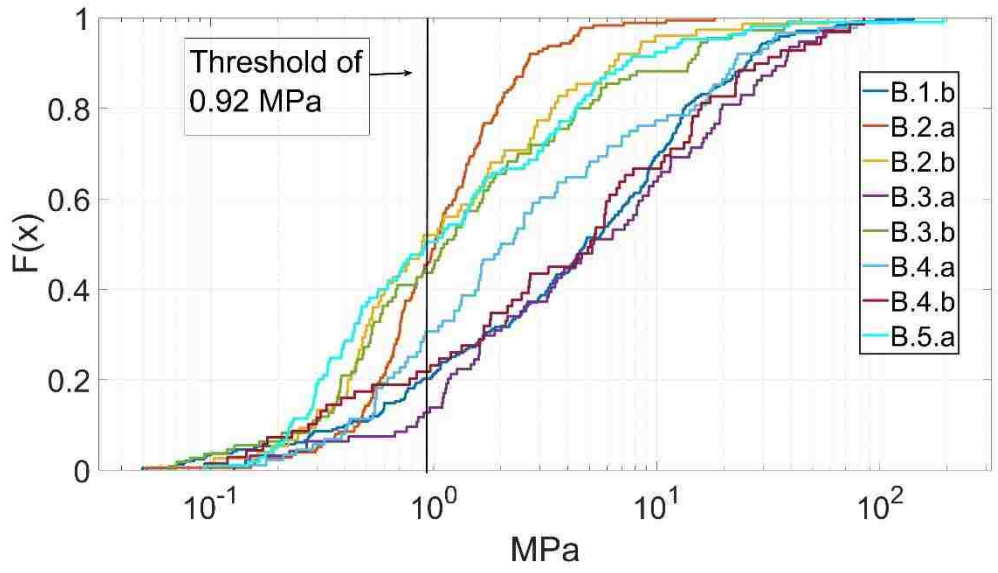

Figure 26. Capillary entry pressure of the wellbore microannuli in all surfaces of wellbore specimen B

3.6.3 Wellbore Specimen C

We found a post-test radial crack that possibly distorted the interpreted hydraulic aperture measured in the flow test. Interpretation of the flowmeter test of wellbore specimen C yielded a hydraulic aperture of 32 µm and we calculated the capillary entry pressure needed to displace the brine (Equation 17), which was 1.44 MPa. Measurements of the actual aperture size allowed us to plot the whole capillary pressure range (Figure 27). Comparison of 1.44 MPa to the CEP of the wellbore specimen C circumferential sections in Figure 27 showed that it was insufficient to push gas through 99% of the apertures of

the microannuli. The cumulative distribution functions of the CEP are almost identical in circumferential sections C.2.a, C.2.b, C.3.b and C.4.b.

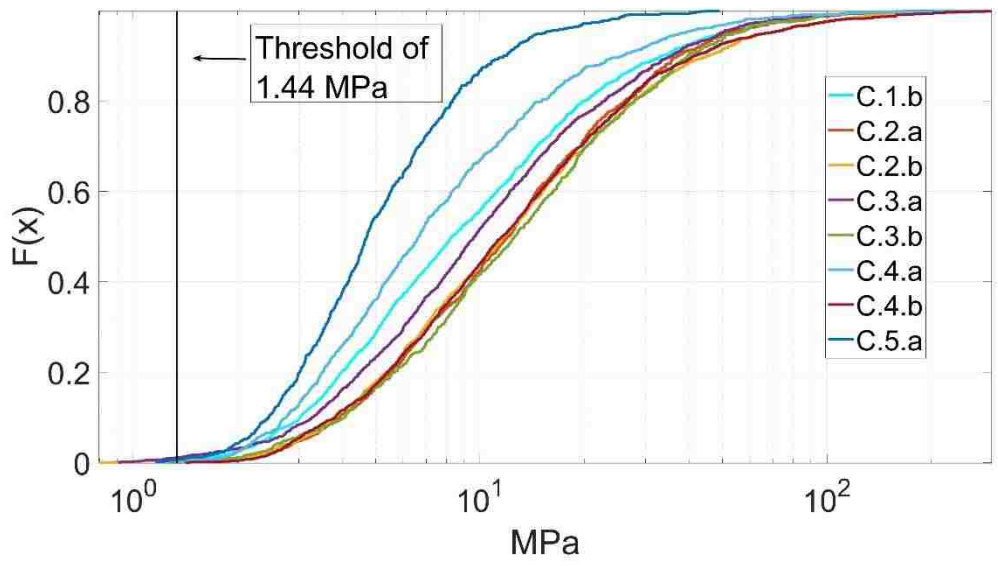

Figure 27. Capillary entry pressure of the wellbore microannuli in all surfaces of wellbore specimen C

3.6.4 General comments

The results shown are dependent on the distribution of aperture size. Furthermore, a single value does not accurately represent the range of capillary entry pressure values for the microannuli. These percentages are calculated on the assumption that the surfaces are perfectly connected. In the likely case that the connectivity is not perfect or that small size values (<15 µm) were to be found along the microannulus, the capillary pressure values could be higher.

3.7 Effective permeability of the samples

The permeability of the wellbore specimens was estimated with flow tests, obtaining an unique value that represents the whole sample. This value, while providing value information, does not describe in detail all the different permeability values of the microannuli. We calculated the permeability for each individual measurement using the equation:

$$k = \frac{h^2}{12} \qquad \text{Equation 18}$$

which is obtained in the derivation of the local cubic law (Equation 1), where K is the permeability of the individual aperture and h is the size of the aperture. Then we compared the flow test calculated permeability with the range of permeabilities of each circumferential section.

3.7.1 Wellbore Specimen A

In Figure 28, we observe the range of permeabilities of apertures in wellbore specimen A. The permeability interpreted from the flowmeter test was $2.06 * 10^{-11}\ m^2$. In this case, the permeability interpreted was smaller than most of the permeability of the apertures measured. More than 95% of the permeability values obtained were greater than those interpreted from the flowmeter test.

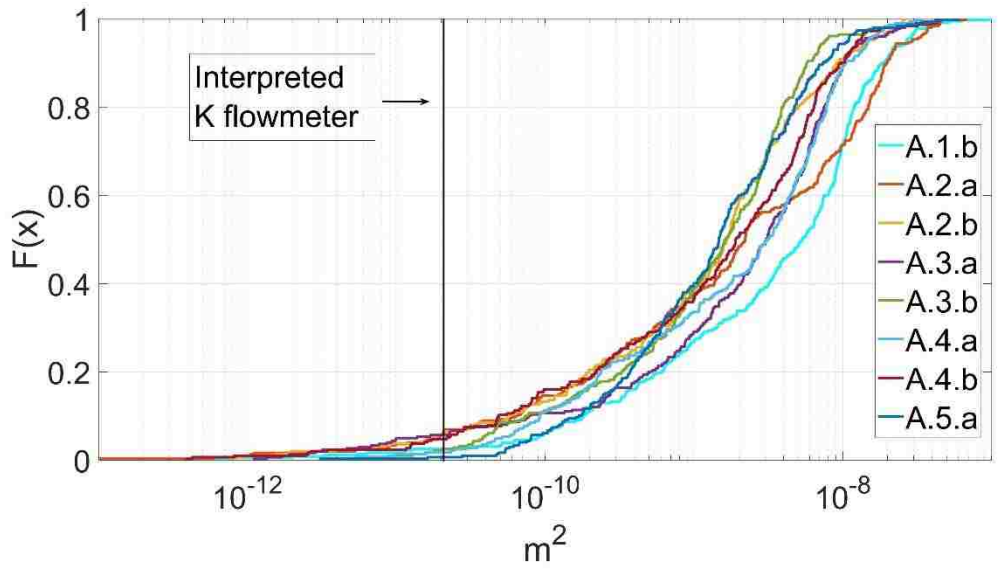

Figure 28. Permeability of wellbore microannuli of all surfaces analyzed in wellbore specimen A

3.7.2 Wellbore Specimen B

The range of permeabilities of the apertures in wellbore specimen B is shown in (Figure 29). The permeability interpreted from the flowmeter test was $4.42 * 10^{-13}$ m^2. Comparing the unique value obtained from the flowmeter to the range of values showed in Figure 29, we found that flowmeter value is smaller than 95% of the permeability values.

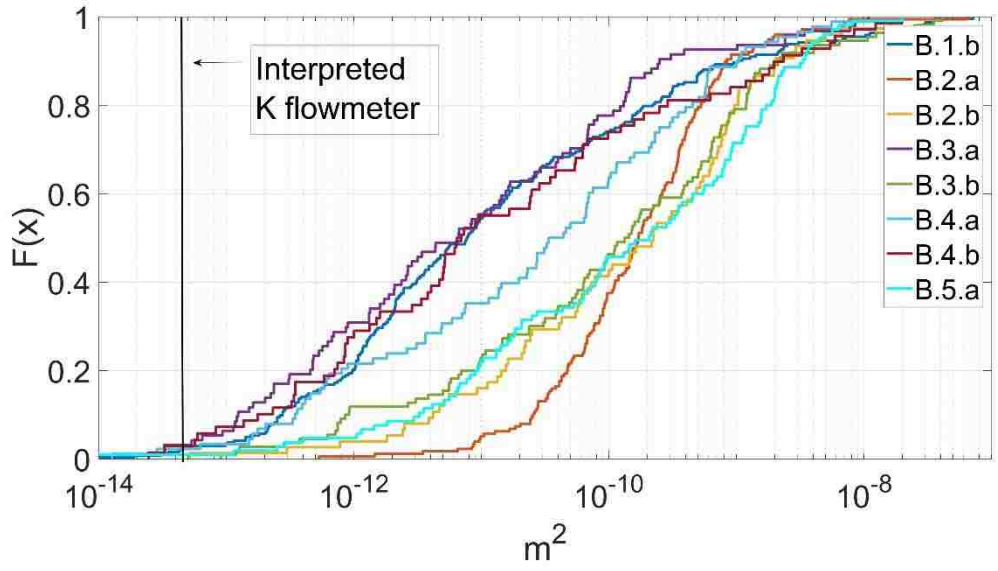

Figure 29. Permeability of the wellbore microannuli of all surfaces analyzed in wellbore specimen B

3.7.3 Wellbore Specimen C

In wellbore specimen C, we detected a post-test radial crack could possibly distort comparison between measured and interpreted apertures from the flow test. Interpretation of the flowmeter test of wellbore specimen C yielded a hydraulic aperture of 32 µm and a permeability of $1.04 * 10^{-13}$ m^2. Comparison of the interpreted value with Figure 30 showed that the apertures will be more conductive at least 88% of the time. In the most favorable section, almost all the apertures are more permeable than the flowmeter value (C.5.a). Six out of eight circumferential sections have apertures (7-12%) that are less permeable. Circumferential sections C.2.a, C.2.b, C.3.b and C.4.b are nearly identical.

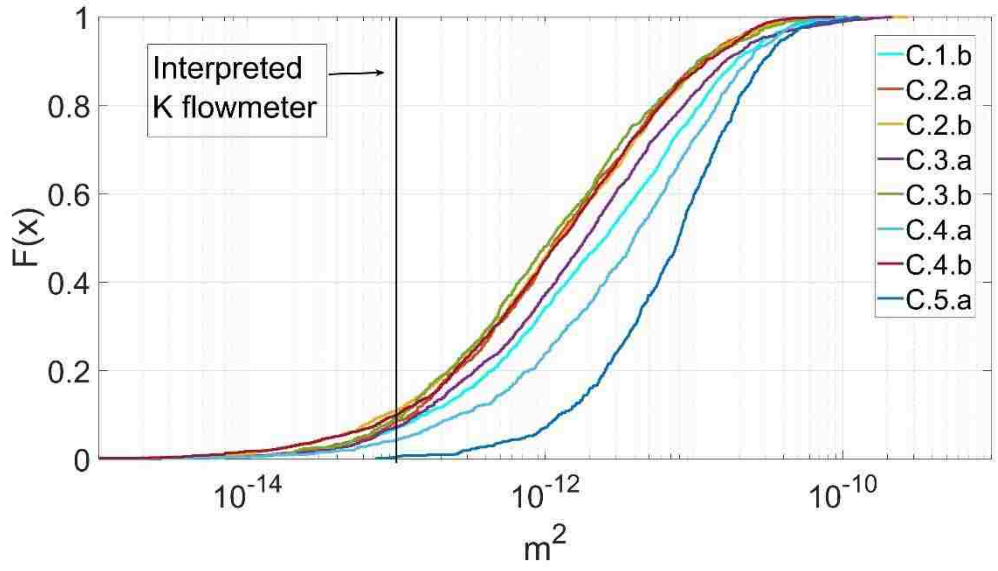

Figure 30. Permeability of the wellbore microannuli of all circumferential sections analyzed in wellbore specimen C

3.7.4 General Comments

We found that the permeabilities interpreted from the flow tests are smaller than the majority of the permeabilities of the apertures measured. This happens because of the assumptions used to obtain the permeability of the flow test: a continuous aperture around the steel casing. The permeability from the test is the permeability of all the cement-steel interface, not just of the microannulus. This means that it is accounting for the locations where there is perfect contact (no microannulus) between the steel and the cement. The range of permeabilities plotted are just of the apertures measured greater than 0; this explains why the permeability of the flow test is in almost every case smaller than 90% of the permeabilities of the microannulus.

3.8 Sealing material performance

Cementitious materials are typically used to repair or enhance the properties of cement, rocks and soils. The purpose of repair is principally to fill voids so as to reduce the permeability of the host material. For an ideal repair, the cementitious material should penetrate and fill all fractures and voids. From a practical standpoint, simply filling interconnected apertures would be sufficient. Penetrability of the repair material in the host material is therefore a critical issue.

Several factors affecting the penetrability of the cement, the most relevant of which are the water/cement ratio and the ratio between the opening size and the grain size of the cement (Axelsson et al., 2009; Jorne and Henriques, 2016; Mirza et al., 2013). With regard to the latter, the generally accepted "rule of thumb" is that the aperture to be filled must be at least three times the grain size of the cement (Mitchell, 1981); this is claimed as a general rule in several reviews (Axelsson et al., 2009; Tolppanen and Syrjänen, 2003). Recent laboratory tests have supported the rule of thumb and have added that, in specific cases under favorable conditions, could be from two to three times smaller than the aperture (Eklund and Stille, 2008). In addition to this rule, different criteria have been proposed that link material grain particle distribution and the aperture of voids. Mitchell found for soils that if the relationship between void size and particle size satisfy (Equation 19), grouting will be successful.

$$\frac{D_{15}^{soil}}{d_{85}^{grout}} > 25 \qquad \text{Equation 19}$$

Where D_{15}^{soil} is the 15th percentile of the size of the voids in the soil and d_{85}^{grout} is the 85th percentile of the size of the cementitious material grain. If the ratio is less than 11, clogging will occur and between 11 and 25, the particles will eventually clog the pathways and the grouting will not completely fill the voids. Miltiadou-Fezans and Tassios, 2013 proposed the use of the minimum nominal width (Equation 20) of the voids to fill and related it to grain particle distribution:

$$W_{nom} = 0.15 * d_{15}^{soil} \quad \text{Equation 20}$$

$$\frac{W_{nom}}{d_{85}} > 4 \; to \; 6 \quad \text{Equation 21}$$

$$\frac{W_{nom}}{d_{99}} > 2 \quad \text{Equation 22}$$

Microannuli apertures are variable and non-uniform, which could complicate the attempt to seal them. If the microannulus is not filled completely, a permeable path may remain that enables fluid migration. The actual repair could be compromised by a low conductivity section. Both problems have been described in detail (Jorne and Henriques, 2016).

We used the criteria presented above to evaluate the repair of the microannuli using different materials. We divided the analysis in two sections; in the first case, we used the

rule of thumb and in the second, we used the different relations presented by Mitchell (Equation 19) and Miltiadou-Fezans and Tassios (Equation 21, Equation 22).

3.8.1 Rule of thumb

On the assumption of perfect connectivity and no plugging nor blockage, we analyzed the aperture size distribution in all three wellbore specimens and estimated the extent to which a microannulus could be repaired and how this would affect specimen permeability. We used three types of cement with distinct maximum grain sizes: standard Portland cement (140 μm), microfine cement (MFC; 30 μm) and ultrafine cement (UFC; 15 μm) (Hansen et al., 2003). Based on the rule of thumb, these cements would not be able to fill any aperture less than 420 μm in the case of Portland cement, 90 μm for MFC and 45 μm for UFC. The results of these analyses are shown in Table 9 and Table 10. Table 9 shows the percentage of the apertures not filled by the repair material and Table 10 shows the percentage of the total permeability that has not been repaired. To obtain Table 10, the individual permeabilities of each measurement were added, obtaining the sum of all of the permeabilities. The individual measurements were then divided by the sum of all, obtaining the individual contribution of each aperture to the total permeability. With these calculations we can obtain the percentage of permeability corresponding to the apertures smaller than 45, 90 and 420 μm.

The aperture measurements of every circumferential section were plotted as cumulative distribution and the three thresholds, one per material, were used to judge the effectiveness (Figure 31, Figure 32, Figure 33).

Wellbore specimen A had an interpreted hydraulic aperture of 175 µm. This information would lead to the expectation that MFC and UFC would repair and fill the apertures, but results suggest that they are not completely filled. We found that MFC would not be able to repair 18-35% of the apertures and UFC 7-18%. Wellbore specimen B had an interpreted hydraulic aperture of 50 µm and UFC penetrates apertures\ up to 45 µm, yet it was found that it is not a perfect repair material for this specimen, since no cementitious material could fill more than 50% of the apertures. In wellbore specimen C, no cementitous paste would be able to repair the microannuli.

These data show that, in general, Portland cement is not suitable for repairing microannuli, and that the variability in aperture size affects their possible repair. An example is wellbore specimen B, which was characterized with an aperture of 50 µm. If a uniform aperture is assumed, it could be considered that UFC would be sufficient to seal it, whereas the apertures measured indicated that, in the best of cases, it would fill only 50% of the microannuli. Changes in the W/C ratio would improve the penetrability, but this factor is not considered in this study.

Since all the circumferential sections differ despite their physical proximity, repair should be dictated by the most restrictive surface in the sample. A cement whose maximum grain size is 5 µm could flow into apertures >15 µm, but given the distribution of the apertures, plugging would be possible due to the substantial number of small apertures. In addition, a sample could have a more restrictive section than those that were analyzed. Aperture connectivity would ultimately affect the repair.

Table 9. Percentage of apertures not filled by the sealing materials.

Material	Wellbore specimen A (%)	Wellbore specimen B (%)	Wellbore specimen C (%)
Regular Cement	78 to 96	95 to 100	100
MFC	20 to 30	65 to 92	100
UFC	5 to 15	50 to 86	99 to 100

Table 10. Percentage of permeability of the surfaces not filled by the sealing material.

Material	Wellbore specimen A (%)	Wellbore specimen B (%)	Wellbore specimen C (%)
Regular Cement	35 to 85	25 to 100	100
MFC	1 to 4	4 to 22	100
UFC	< 1	1 to 5	85 to 100

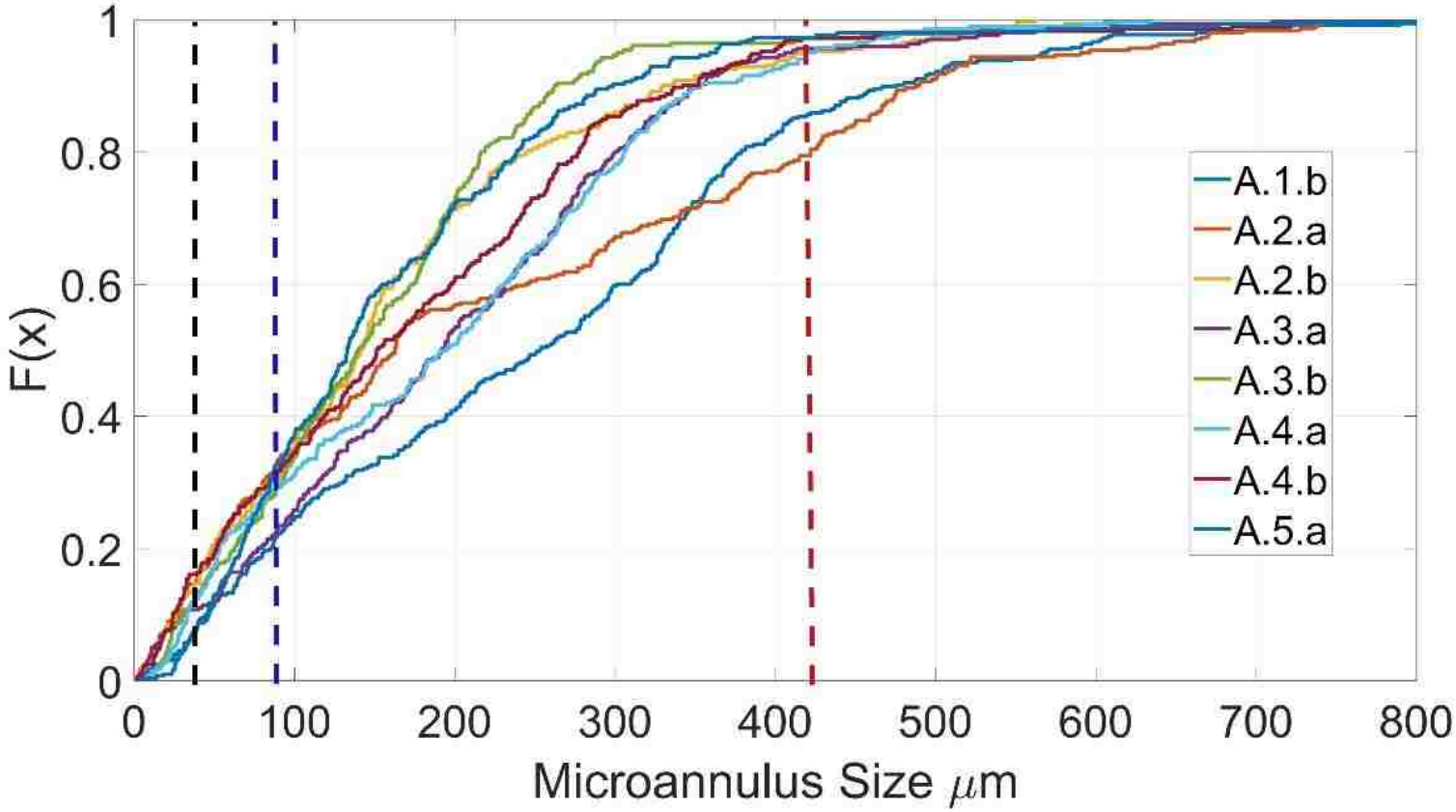

Figure 31. Cumulative frequency distribution of all surfaces of wellbore specimen A. The dash lines represent the threshold of reparation using the rule of thumb of UFC (black), MFC (blue) and Portland cement (red).

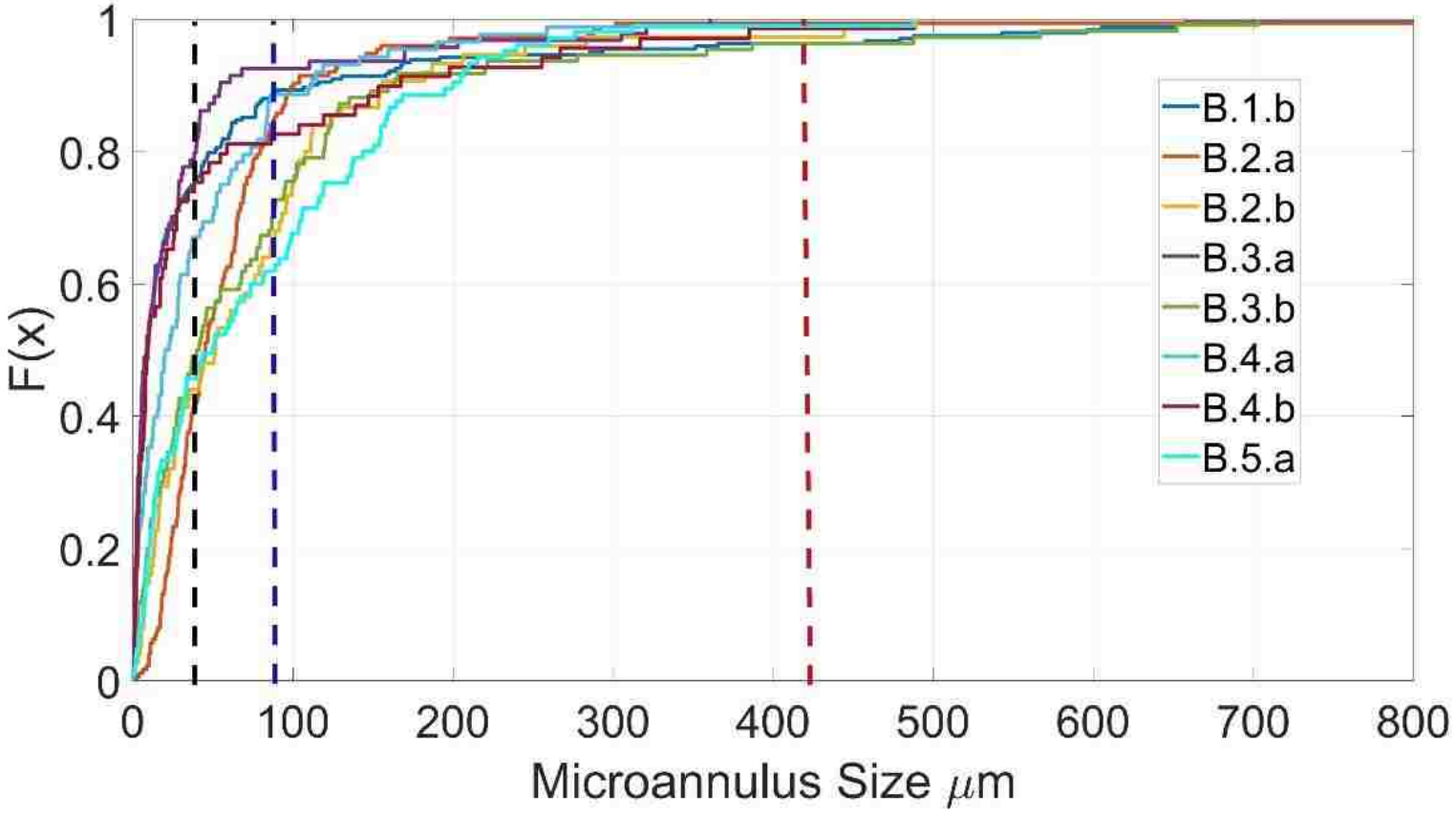

Figure 32. Cumulative frequency distribution of all surfaces of wellbore specimen B. The dash lines represent the threshold of reparation using the rule of thumb of UFC (black), MFC (blue) and Portland cement (red).

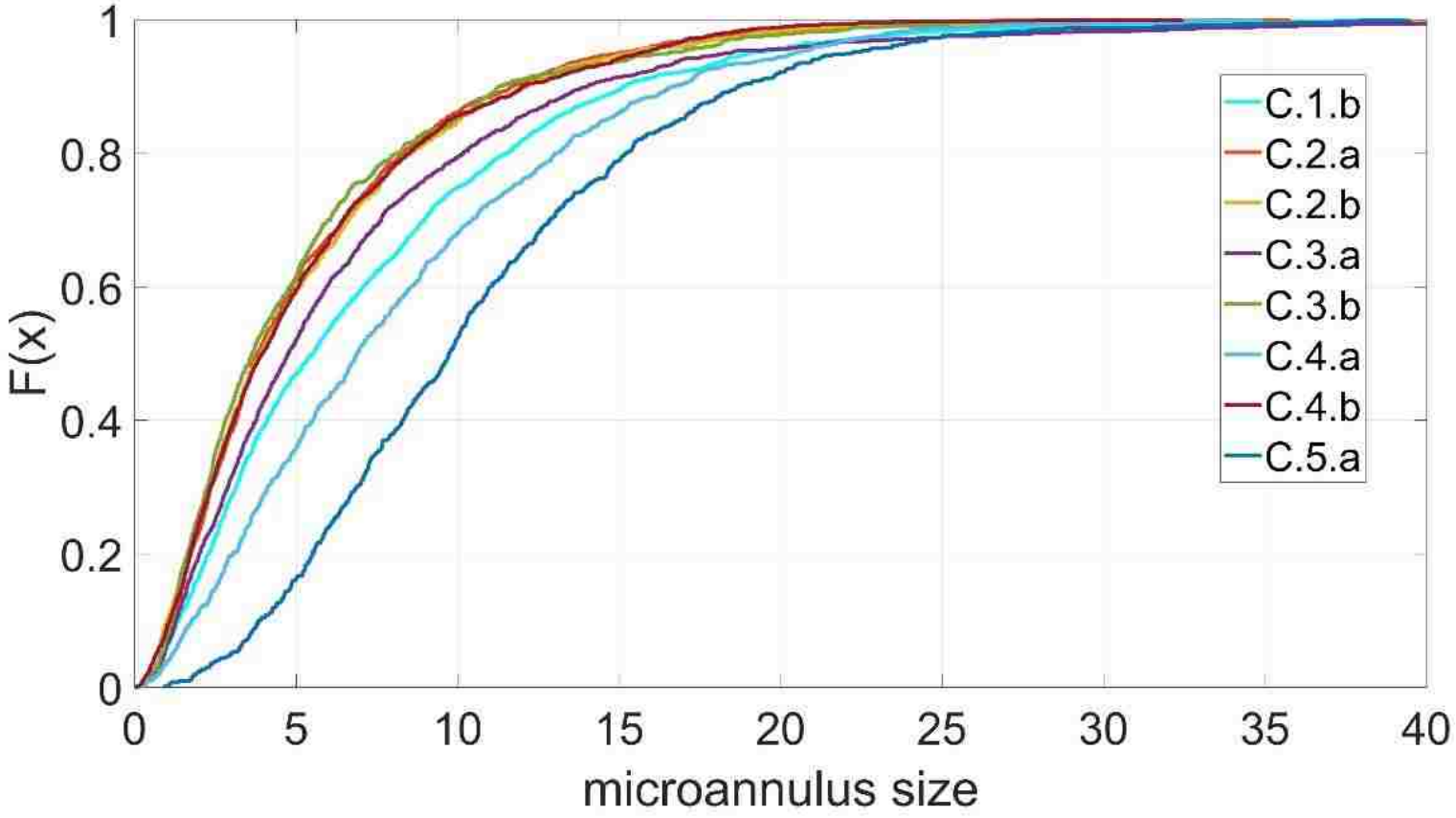

Figure 33. Cumulative frequency distribution of all surfaces of wellbore specimen C. Aperture sizes are too small to plot the repair materials.

3.8.2 Grain size/void ratios

To evaluate other penetrability citeria, the complete particle size distribution of the cementitious materials is required. Mirza et al. (Mirza et al., 2013) provide the grain size distribution of two standard Portland cements and seven commercial microfine cements. We added De Neef MC-500, labeled as "microfine cement 8" since it provided a finer granulometry than the previous seven. The d_{85} and d_{99} of the cementitious materials are presented in chart (Table 11), representing a range of granulometries from Portland cement to microfine cement.

Table 11. Particle size (µm) of the cementitious materials indicated by Mirza et al., 2013 and MC-500, necessary for calculation of the ratios proposed by Miltiadou-Fezans and Tassios, 2013 and by Mitchell, 1981.

	d_{85} (µm)	d_{99} (µm)
Portland Cement 1	37	100
Portland Cement 2	26	65
Microfine Cement 1	17	65
Microfine Cement 2	11	32
Microfine Cement 3	10	23
Microfine Cement 4	9	20

Microfine Cement 5	6	15
Microfine Cement 6	8	20
Microfine Cement 7	7	22
Microfine Cement 8	6	11

The criteria cited in this section were originally proposed for different soils, but from our experimental data, we have seen that microannuli have the same issues in terms of penetrability (void/aperture size distribution and connectivity (Jorne and Henriques, 2016). W_{nom} and D_{15}^{soil} were calculated for microannuli (Equation 19, Equation 20, Equation 21) using the aperture size distributions obtained from the circumferential section. The ratios were applied independently to each section of the wellbore specimens (Table 12, Table 13 , Table 14). No circumferential section of the three specimens passed any of the three different criteria set (Equation 19, Equation 21, Equation 22). This finding does not mean that some of the microfine cements tested could fill some apertures partially, but they would not fill and completely repair the microannuli.

Table 12. Wellbore Specimen A tested for the three criteria. No circumferential section passed the groutability injection threshold.

$\frac{D_{15}^{ma}}{d_{85}^{grout}} > 25$	1.b	2.a	2.b	3.a	3.b	4.a	4.b	5.a
Portland Cement 1	1.74	1.04	1.10	1.55	1.19	1.23	0.88	1.49
Portland Cement 2	2.48	1.48	1.57	2.21	1.70	1.74	1.26	2.11
Microfine Cement 1	3.79	2.26	2.40	3.37	2.60	2.67	1.92	3.23
Microfine Cement 2	5.85	3.49	3.70	5.22	4.02	4.12	2.97	5.00
Microfine Cement 3	6.44	3.84	4.07	5.74	4.42	4.54	3.27	5.50
Microfine Cement 4	7.15	4.26	4.53	6.37	4.91	5.04	3.63	6.11
Microfine Cement 5	10.73	6.39	6.79	9.56	7.37	7.56	5.45	9.16
Microfine Cement 6	8.05	4.80	5.09	7.17	5.53	5.67	4.09	6.87
Microfine Cement 7	9.20	5.48	5.82	8.20	6.31	6.48	4.67	7.85
Microfine Cement 8	10.73	6.39	6.79	9.56	7.37	7.56	5.45	9.16
$\frac{W_{nom}}{d_{85}} > 4$ to 6	1.b	2.a	2.b	3.a	3.b	4.a	4.b	5.a
Portland Cement 1	0.26	0.16	0.17	0.23	0.18	0.18	0.13	0.22
Portland Cement 2	0.37	0.22	0.23	0.33	0.26	0.26	0.19	0.32
Microfine Cement 1	0.57	0.34	0.36	0.51	0.39	0.40	0.29	0.48
Microfine Cement 2	0.88	0.52	0.56	0.78	0.60	0.62	0.45	0.75
Microfine Cement 3	0.97	0.58	0.61	0.86	0.66	0.68	0.49	0.82
Microfine Cement 4	1.07	0.64	0.68	0.96	0.74	0.76	0.55	0.92

Microfine Cement 5	1.61	0.96	1.02	1.43	1.11	1.13	0.82	1.37
Microfine Cement 6	1.21	0.72	0.76	1.08	0.83	0.85	0.61	1.03
Microfine Cement 7	1.38	0.82	0.87	1.23	0.95	0.97	0.70	1.18
Microfine Cement 8	1.61	0.96	1.02	1.43	1.11	1.13	0.82	1.37
$\frac{W_{nom}}{d_{99}} > 2$	1.b	2.a	2.b	3.a	3.b	4.a	4.b	5.a
Portland Cement 1	0.10	0.06	0.06	0.09	0.07	0.07	0.05	0.08
Portland Cement 2	0.15	0.09	0.09	0.13	0.10	0.10	0.08	0.13
Microfine Cement 1	0.15	0.09	0.09	0.13	0.10	0.10	0.08	0.13
Microfine Cement 2	0.30	0.18	0.19	0.27	0.21	0.21	0.15	0.26
Microfine Cement 3	0.42	0.25	0.27	0.37	0.29	0.30	0.21	0.36
Microfine Cement 4	0.48	0.29	0.31	0.43	0.33	0.34	0.25	0.41
Microfine Cement 5	0.64	0.38	0.41	0.57	0.44	0.45	0.33	0.55
Microfine Cement 6	0.48	0.29	0.31	0.43	0.33	0.34	0.25	0.41
Microfine Cement 7	0.44	0.26	0.28	0.39	0.30	0.31	0.22	0.37
Microfine Cement 8	0.88	0.52	0.56	0.78	0.60	0.62	0.45	0.75

Table 13. Wellbore Specimen B tested for the three criteria. No circumferential section passed the groutability injection threshold.

$\frac{D_{15}^{ma}}{d_{85}^{grout}} > 25$	1.b	2.a	2.b	3.a	3.b	4.a	4.b	5.a
Portland Cement 1	0.06	0.54	0.22	0.04	0.21	0.06	0.05	0.24
Portland Cement 2	0.09	0.77	0.31	0.06	0.30	0.09	0.08	0.33
Microfine Cement 1	0.14	1.17	0.48	0.10	0.46	0.14	0.12	0.51
Microfine Cement 2	0.21	1.81	0.74	0.15	0.70	0.21	0.18	0.79
Microfine Cement 3	0.23	2.00	0.82	0.16	0.77	0.23	0.20	0.87
Microfine Cement 4	0.26	2.22	0.91	0.18	0.86	0.26	0.22	0.97
Microfine Cement 5	0.38	3.33	1.36	0.27	1.29	0.39	0.34	1.45
Microfine Cement 6	0.29	2.50	1.02	0.20	0.97	0.29	0.25	1.09
Microfine Cement 7	0.33	2.85	1.17	0.23	1.11	0.33	0.29	1.24
Microfine Cement 8	0.38	3.33	1.36	0.27	1.29	0.39	0.34	1.45
$\frac{W_{nom}}{d_{85}} > 4$ to 6	1.b	2.a	2.b	3.a	3.b	4.a	4.b	5.a
Portland Cement 1	0.01	0.08	0.03	0.01	0.03	0.01	0.01	0.04
Portland Cement 2	0.01	0.12	0.05	0.01	0.04	0.01	0.01	0.05
Microfine Cement 1	0.02	0.18	0.07	0.01	0.07	0.02	0.02	0.08
Microfine Cement 2	0.03	0.27	0.11	0.02	0.11	0.03	0.03	0.12
Microfine Cement 3	0.03	0.30	0.12	0.02	0.12	0.04	0.03	0.13
Microfine Cement 4	0.04	0.33	0.14	0.03	0.13	0.04	0.03	0.14

Microfine Cement 5	0.06	0.50	0.20	0.04	0.19	0.06	0.05	0.22
Microfine Cement 6	0.04	0.37	0.15	0.03	0.15	0.04	0.04	0.16
Microfine Cement 7	0.05	0.43	0.17	0.04	0.17	0.05	0.04	0.19
Microfine Cement 8	0.06	0.50	0.20	0.04	0.19	0.06	0.05	0.22
$\frac{W_{nom}}{d_{99}} > 2$	1.b	2.a	2.b	3.a	3.b	4.a	4.b	5.a
Portland Cement 1	0.00	0.03	0.01	0.00	0.01	0.00	0.00	0.01
Portland Cement 2	0.01	0.05	0.02	0.00	0.02	0.01	0.00	0.02
Microfine Cement 1	0.01	0.05	0.02	0.00	0.02	0.01	0.00	0.02
Microfine Cement 2	0.01	0.09	0.04	0.01	0.04	0.01	0.01	0.04
Microfine Cement 3	0.01	0.13	0.05	0.01	0.05	0.02	0.01	0.06
Microfine Cement 4	0.02	0.15	0.06	0.01	0.06	0.02	0.02	0.07
Microfine Cement 5	0.02	0.20	0.08	0.02	0.08	0.02	0.02	0.09
Microfine Cement 6	0.02	0.15	0.06	0.01	0.06	0.02	0.02	0.07
Microfine Cement 7	0.02	0.14	0.06	0.01	0.05	0.02	0.01	0.06
Microfine Cement 8	0.03	0.27	0.11	0.02	0.11	0.03	0.03	0.12

Table 14. Wellbore Specimen C tested for the three criteria. No circumferential section passed the groutability injection threshold.

$\frac{D_{15}^{ma}}{d_{85}^{grout}} > 25$	1.b	2.a	2.b	3.a	3.b	4.a	4.b	5.a
Portland Cement 1	0.05	0.04	0.04	0.04	0.07	0.13	0.04	0.04
Portland Cement 2	0.07	0.06	0.06	0.05	0.10	0.19	0.05	0.06
Microfine Cement 1	0.11	0.09	0.10	0.08	0.15	0.28	0.08	0.09
Microfine Cement 2	0.17	0.14	0.15	0.12	0.23	0.44	0.12	0.13
Microfine Cement 3	0.18	0.15	0.16	0.14	0.25	0.48	0.13	0.15
Microfine Cement 4	0.20	0.17	0.18	0.15	0.28	0.54	0.15	0.16
Microfine Cement 5	0.30	0.25	0.27	0.23	0.42	0.80	0.22	0.24
Microfine Cement 6	0.23	0.19	0.20	0.17	0.31	0.60	0.17	0.18
Microfine Cement 7	0.26	0.21	0.23	0.19	0.36	0.69	0.19	0.21
Microfine Cement 8	0.30	0.25	0.27	0.23	0.42	0.80	0.22	0.24
$\frac{W_{nom}}{d_{85}} > 4$ to 6	1.b	2.a	2.b	3.a	3.b	4.a	4.b	5.a
Portland Cement 1	0.01	0.01	0.01	0.01	0.01	0.02	0.01	0.01
Portland Cement 2	0.01	0.01	0.01	0.01	0.01	0.03	0.01	0.01
Microfine Cement 1	0.02	0.01	0.01	0.01	0.02	0.04	0.01	0.01
Microfine Cement 2	0.02	0.02	0.02	0.02	0.03	0.07	0.02	0.02
Microfine Cement 3	0.03	0.02	0.02	0.02	0.04	0.07	0.02	0.02
Microfine Cement 4	0.03	0.02	0.03	0.02	0.04	0.08	0.02	0.02

Microfine Cement 5	0.05	0.04	0.04	0.03	0.06	0.12	0.03	0.04
Microfine Cement 6	0.03	0.03	0.03	0.03	0.05	0.09	0.03	0.03
Microfine Cement 7	0.04	0.03	0.03	0.03	0.05	0.10	0.03	0.03
Microfine Cement 8	0.05	0.04	0.04	0.03	0.06	0.12	0.03	0.04
$\frac{W_{nom}}{d_{99}} > 2$	1.b	2.a	2.b	3.a	3.b	4.a	4.b	5.a
Portland Cement 1	0.00	0.00	0.00	0.00	0.00	0.01	0.00	0.00
Portland Cement 2	0.00	0.00	0.00	0.00	0.01	0.01	0.00	0.00
Microfine Cement 1	0.00	0.00	0.00	0.00	0.01	0.01	0.00	0.00
Microfine Cement 2	0.01	0.01	0.01	0.01	0.01	0.02	0.01	0.01
Microfine Cement 3	0.01	0.01	0.01	0.01	0.02	0.03	0.01	0.01
Microfine Cement 4	0.01	0.01	0.01	0.01	0.02	0.04	0.01	0.01
Microfine Cement 5	0.02	0.01	0.02	0.01	0.03	0.05	0.01	0.01
Microfine Cement 6	0.01	0.01	0.01	0.01	0.02	0.04	0.01	0.01
Microfine Cement 7	0.01	0.01	0.01	0.01	0.02	0.03	0.01	0.01
Microfine Cement 8	0.02	0.02	0.02	0.02	0.03	0.07	0.02	0.02

4. Conclusions

Using microphotography we have shown that the microannuli produced in laboratory wellbore samples have a wide range of apertures; we observed apertures that varied orders of magnitude in a circumferential section. In addition, in portions of the wellbore specimens, there is contact between the steel and the cement. This complex geometry results in tortuous flow paths, far from the assumption of flow between parallel plates often used to describe flow through microannuli.

The aforementioned geometry makes difficult to obtain a relation between the hydraulic apertures, obtained using the local cubic law in flow tests, and the mechanical apertures. Fitting the aperture data to statistical distributions helped generalize and quantify aperture sizes. We used statistical distributions that were reported in literature as fracture aperture size distribution of different rocks under different stress conditions. We fit the aperture data from every circumferential section of each wellbore specimen and all the data of each wellbore specimen together to various distributions.

We tested wellbore specimens A, B and C. The microannuli of wellbore specimens A and B was created using a release film and microannuli of wellbore specimen C was created by thermal debonding. The microannuli of A was bigger than B and b was bigger than C. We found that the circumferential sections of wellbore specimens A are not as consistent as the circumferential sections of wellbore specimens B and C, which are generally well-fit by lognormal and generalized gamma distributions, especially with the modified forms of these distributions. While fitting all the data of each specimen together we found that

both wellbore specimens A and B fit the generalized gamma 4P distribution. Wellbore specimen C does not fit any distribution in large part because of the large number of data points, but we have shown that a generalized gamma 4P will be a good approximation for a dataset of over 10000 points.

It was also found using the Pearson correlation coefficient that the apertures were not correlated vertically along the axis of the wellbore specimen. Only the apertures of wellbore specimen A had a horizontal correlation. Along the vertical axis, we calculated the continuous flow paths and the continuous contact by extrapolating between sections where apertures were measured. These calculations showed that the fluid moving along the wellbore axis will travel a tortuous path and that some parts of the specimens do not contribute at all in the flow. In addition, consecutive circumferential sections, even the ones separated just by the thickness of the blade used to section the specimen, do not come from the same statistical distribution (as determined from the Kolmogorov-Smirnoff 2-test).

A convergence study was conducted to find how many circumferential sections are necessary to provide a reasonable representation of the entire sample. The results indicate that, while the characteristics of each circumferential section vary, most parameters are within a relatively small range. This means that despite the fact that the microannuli vary throughout the specimens, measuring a single circumferential section will provide meaningful information for the entire sample. A second convergence study investigated the degree of discretization of the aperture along a circumferential section. Insufficient discretization, that is, making too few measurements will yield in

misrepresentation of the geometry, and the interpreted hydraulic aperture will be clearly underestimated.

The comparison of the interpreted hydraulic aperture from the flow tests and the interpreted apertures obtained using the imaging technique showed that the mechanical mean of the apertures measured, not including the zero values (contact), is the nearest value in wellbore specimens A and B. The local cubic law provides a reasonable first order approximation, but it seems to overestimate the hydraulic apertures. In wellbore specimen C we found a post-test radial crack, which makes it difficult to compare results.

We did not find any relation between the physical position of the circumferential sections and the aperture sizes found. One hypothesis was that, due to gravity, the apertures would be smaller as we move from the top to the bottom of the wellbore specimens. While this could be envisioned to occur under some conditions, this was not observed on our samples.

Using data from the imaging technique, we calculated the capillary entry pressure of each individual aperture, assuming the apertures were filled with brine and CO_2 was trying to flow through. This resulted in a wide range of pressures (2 orders of magnitude) along a circumferential section, where the capillary entry pressure interpreted from the flow test fall in between these ranges.

The range of permeabilities calculated in each circumferential section showed that the individual permeabilities of each aperture are bigger than the interpreted permeability from the flow test of the specimen. This is explained by the fact that the permeability

from the flow test is an average of the whole sample, including the parts with perfect contact and the cement itself.

The aperture measurements were used to evaluate the possibility of a repair using cementitious materials. Several criteria were used, but all of them showed that it was not possible to fully repair the microannulus since it has apertures too small for cementitious material to fill (<50μm). Furthermore, partial repair could be performed, but, for an interpreted hydraulic aperture of 50 μm (wellbore specimen B) we found that 50-86% of the microannuli will remain unfilled with cementitious material.

Future research

One of the limitations of the imaging technique used is, as it was explained in the materials and methods section, the fact that the measurements are not continuous throughout the steel casing axis. CT scan can provide more continuous measurements, but for the size of our specimens the resolutions was too low. A new possibility could be to produce smaller scaled specimens where the microannuli is created in a realistic manner. If possible, using representative temperature and pressure underground values. Studies of the spatial correlation of the apertures of the microannuli, combined with statistical distributions of the apertures of the microannuli would be a valuable dataset.

Appendix A

The code implemented to improve the photomerge in Photoshop:

```
// Functions
function savePSB( filePath ) {
	function cTID(s) { return app.charIDToTypeID(s); };
	//function sTID(s) { return app.stringIDToTypeID(s); };

	var desc7 = new ActionDescriptor();
	var desc8 = new ActionDescriptor();
	desc7.putObject( cTID('As  '), cTID('Pht8'), desc8 );
	desc7.putPath( cTID('In  '), new File( filePath ) );
	desc7.putBoolean( cTID('LwCs'), true );
	executeAction( cTID('save'), desc7, DialogModes.NO );
};

function padNumerito(num, size) {
	var s = num+"";
	while (s.length < size) s = "0" + s;
	return s;
}

// Import Photomerge
	var runphotomergeFromScript = true; // must be before Photomerge include

	// Option 1
	/*
```

```
        // @includepath “/c/Program Files/Adobe/Adobe Photoshop CS4 (64 Bit)/Presets/Scripts/”

        // @include “Photomerge.jsx”

        // @show include

        */


        // Option 2

        $.evalFile( app.path + "/Presets/Scripts/Photomerge.jsx");

        //alert(app.path);

        //$.evalFile( "C:/Program Files/Adobe/Adobe Photoshop CC 2017/Presets/Scripts/Photomerge.jsx");



// photomarge config

        // override Photomerge.jsx settings. Default is "Auto". Uncomment to override the default.

        //photomerge.alignmentKey   = "Auto";

        //photomerge.alignmentKey   = "Prsp";

        //photomerge.alignmentKey   = "cylindrical";

        //photomerge.alignmentKey   = "spherical";

        //photomerge.alignmentKey   = "sceneCollage";

        photomerge.alignmentKey   = "translation"; // "Reposition" in layout dialog

        // other setting that may need to be changed. Defaults below

        photomerge.advancedBlending      = true; // 'Bend Images Together' checkbox in dialog

        photomerge.lensCorrection      = false; // Geometric Distortion Correction'checkbox in dialog

        photomerge.removeVignette      = true; // 'Vignette Removal' checkbox in dialog
```

```
// Saving Options
	psdOpts = new PhotoshopSaveOptions();
	psdOpts.embedColorProfile = true;
	psdOpts.alphaChannels = true;
	psdOpts.layers = true;


// --------------------Stitching----------------------------------------

var folderPath = "e:/reich";

var folder = new Folder(folderPath + "/imagenes/");


var fList = folder.getFiles( '*.psb' );
fList.sort(function(a, b) {
	return (a < b) ? -1 : (a > b) ? 1 : 0;
});

photomerge.createPanorama(fList,false);

// The merged doc will be the activeDocument
savePSB(folderPath + "/Stitch.psb");
activeDocument.close( SaveOptions.DONOTSAVECHANGES );
```

References

Akhavan, A., Shafaatian, S.-M.-H., Rajabipour, F., 2012. Quantifying the effects of crack width, tortuosity, and roughness on water permeability of cracked mortars. Cem. Concr. Res. 42, 313–320. https://doi.org/10.1016/j.cemconres.2011.10.002

Andrew, M., Bijeljic, B., Blunt, M.J., 2013. Pore-scale imaging of geological carbon dioxide storage under in situ conditions. Geophys. Res. Lett. 40, 3915–3918. https://doi.org/10.1002/grl.50771

API, A.P.I. (2 9). "Specification for Cements and Materials for Well Cementing." API Specification 10A: American Petroleum Institute, Washington, DC.

Asadollahi, P., 2009. Stability analysis of a single three dimensional rock block: effect of dilatancy and high-velocity water jet impact.

ASTM, A., 2014. 305-14 Standard practice for mechanical mixing of hydraulic cement pastes and mortars of plastic consistency ASTM C305-14. ASTM Int. West Conshohocken PA.

Axelsson, M., Gustafson, G., Fransson, Å., 2009. Stop mechanism for cementitious grouts at different water-to-cement ratios. Tunn. Undergr. Space Technol. 24, 390–397. https://doi.org/10.1016/j.tust.2008.11.001

Bachu, S., 2013. Drainage and Imbibition CO2/Brine Relative Permeability Curves at in Situ Conditions for Sandstone Formations in Western Canada. Energy Procedia, GHGT-11 Proceedings of the 11th International Conference on Greenhouse Gas Control Technologies, 18-22 November 2012, Kyoto, Japan 37, 4428–4436. https://doi.org/10.1016/j.egypro.2013.07.001

Bachu, S., Bennion, D.B., 2009. Experimental assessment of brine and/or CO2 leakage through well cements at reservoir conditions. Int. J. Greenh. Gas Control 3, 494–501. https://doi.org/10.1016/j.ijggc.2008.11.002

Barlet-Gouedard, V., Rimmele, G., Goffe, B., Porcherie, O., 2006. Mitigation strategies for the risk of CO2 migration through wellbores. Presented at the IADC/SPE Drilling Conference, Society of Petroleum Engineers. https://doi.org/10.2118/98924-MS

Barton, C.C., Hsieh, P.A., 1989. Physical and hydrologic-flow properties of fractures, in: 28th International Geological Congress Field Trip Guidebook. p. 36.

Bellabarba, M., Bulte-Loyer, H., Froelich, B., Le Roy-Delage, S., van Kuijk, R., Zeroug, S., Guillot, D., Moroni, N., Pastor, S., Zanchi, A., 2008. Ensuring zonal isolation beyond the life of the well. Oilfield Rev. 20, 18–31.

Bertels, S.P., DiCarlo, D.A., Blunt, M.J., 2001. Measurement of aperture distribution, capillary pressure, relative permeability, and in situ saturation in a rock fracture using computed tomography scanning. Water Resour. Res. 37, 649–662. https://doi.org/10.1029/2000WR900316

Bianchi, L., Snow, D.T., 1969. Permeability of crystalline rock interpreted from measured orientations and apertures of fractures.

Bielicki, J.M., Pollak, M.F., Fitts, J.P., Peters, C.A., Wilson, E.J., 2014. Causes and financial consequences of geologic CO2 storage reservoir leakage and interference with other subsurface resources. Int. J. Greenh. Gas Control 20, 272–284. https://doi.org/10.1016/j.ijggc.2013.10.024

Blunt, M.J., 2017. Multiphase Flow in Permeable Media: A Pore-Scale Perspective. Cambridge University Press.

Bois, A.-P., Garnier, A., Rodot, F., Sain-Marc, J., Aimard, N., others, 2011. How to prevent loss of zonal isolation through a comprehensive analysis of microannulus formation. SPE Drill. Complet. 26, 13–31.

Boukhelifa, L., Moroni, N., James, S.G., Le Roy-Delage, S., Thiercelin, M.J., Lemaire, G., 2004. Evaluation of cement systems for oil and gas well zonal isolation in a full-scale annular geometry. Presented at the IADC/SPE Drilling Conference, Society of Petroleum Engineers. https://doi.org/10.2118/87195-MS

Brown, S.R., 1987. Fluid flow through rock joints: The effect of surface roughness. J. Geophys. Res. Solid Earth 92, 1337–1347. https://doi.org/10.1029/JB092iB02p01337

Carey, J.W., Lewis, K., Kelkar, S., Zyvoloski, G.A., 2013. Geomechanical Behavior of Wells in Geologic Sequestration. Energy Procedia, GHGT-11 Proceedings of the 11th International Conference on Greenhouse Gas Control Technologies, 18-22 November 2012, Kyoto, Japan 37, 5642–5652. https://doi.org/10.1016/j.egypro.2013.06.486

Carey, J.W., Svec, R., Grigg, R., Zhang, J., Crow, W., 2010. Experimental investigation of wellbore integrity and CO 2–brine flow along the casing–cement microannulus. Int. J. Greenh. Gas Control 4, 272–282.

Carey, J.W., Wigand, M., Chipera, S.J., WoldeGabriel, G., Pawar, R., Lichtner, P.C., Wehner, S.C., Raines, M.A., Guthrie, G.D., 2007. Analysis and performance of

oil well cement with 30 years of CO 2 exposure from the SACROC Unit, West Texas, USA. Int. J. Greenh. Gas Control 1, 75–85.

Carroll, S.A., Keating, E., Mansoor, K., Dai, Z., Sun, Y., Trainor-Guitton, W., Brown, C., Bacon, D., 2014. Key factors for determining groundwater impacts due to leakage from geologic carbon sequestration reservoirs. Int. J. Greenh. Gas Control 29, 153–168. https://doi.org/10.1016/j.ijggc.2014.07.007

Checkai, D., Bryant, S., Tao, Q., 2013. Towards a frequency distribution of effective permeabilities of leaky wellbores. Energy Procedia, GHGT-11 Proceedings of the 11th International Conference on Greenhouse Gas Control Technologies, 18-22 November 2012, Kyoto, Japan 37, 5653–5660. https://doi.org/10.1016/j.egypro.2013.06.487

Checkai, D.A., 2012. Estimating permeability distribution of leakage pathways along existing wellbores (thesis).

Chiquet, P., Daridon, J.-L., Broseta, D., Thibeau, S., 2007. CO2/water interfacial tensions under pressure and temperature conditions of CO2 geological storage. Energy Convers. Manag. 48, 736–744. https://doi.org/10.1016/j.enconman.2006.09.011

Crandall, D., Bromhal, G., Karpyn, Z.T., 2010. Numerical simulations examining the relationship between wall-roughness and fluid flow in rock fractures. Int. J. Rock Mech. Min. Sci. 47, 784–796. https://doi.org/10.1016/j.ijrmms.2010.03.015

Crow, W., Carey, J.W., Gasda, S., Brian Williams, D., Celia, M.A., 2010. Wellbore integrity analysis of a natural CO_2producer. Int. J. Greenh. Gas Control, The Ninth International Conference on Greenhouse Gas Control Technologies 4, 186–197. https://doi.org/10.1016/j.ijggc.2009.10.010

Davies, R.J., Almond, S., Ward, R.S., Jackson, R.B., Adams, C., Worrall, F., Herringshaw, L.G., Gluyas, J.G., Whitehead, M.A., 2014. Oil and gas wells and their integrity: Implications for shale and unconventional resource exploitation. Mar. Pet. Geol. 56, 239–254. https://doi.org/10.1016/j.marpetgeo.2014.03.001

Deng, H., Ellis, B.R., Peters, C.A., Fitts, J.P., Crandall, D., Bromhal, G.S., 2013. Modifications of Carbonate Fracture Hydrodynamic Properties by CO2-Acidified Brine Flow. Energy Fuels 27, 4221–4231. https://doi.org/10.1021/ef302041s

Diez, D.M., Barr, C.D., Çetinkaya-Rundel, M., 2015. OpenIntro Statistics. OpenIntro, Incorporated.

Duguid, A., Carey, J.W., Butsch, R., 2014. Well Integrity Assessment of a 68 year old Well at a CO2 Injection Project. Energy Procedia, 12th International Conference on Greenhouse Gas Control Technologies, GHGT-12 63, 5691–5706. https://doi.org/10.1016/j.egypro.2014.11.602

Duguid, A., Scherer, G.W., 2010. Degradation of oilwell cement due to exposure to carbonated brine. Int. J. Greenh. Gas Control 4, 546–560. https://doi.org/10.1016/j.ijggc.2009.11.001

Dusseault, M.B., Jackson, R.E., Macdonald, D., 2014. Towards a road map for mitigating the rates and occurrences of long-term wellbore leakage. Univ. Waterloo Geofirma Eng. LTD.

Eklund, D., Stille, H., 2008. Penetrability due to filtration tendency of cement-based grouts. Tunn. Undergr. Space Technol. 23, 389–398. https://doi.org/10.1016/j.tust.2007.06.011

Ficker, T., Martišek, D., Jennings, H.M., 2010. Roughness of fracture surfaces and compressive strength of hydrated cement pastes. Cem. Concr. Res. 40, 947–955. https://doi.org/10.1016/j.cemconres.2010.02.002

Forchheimer, P.H., 1901. Wasserbewegung durch boden. Zeitz Ver Duetch Ing 45, 1782–1788.

Gale, J.E., 1987. Comparison of coupled fracture deformation and fluid flow models with direct measurements of fracture pore structure and stress-flow properties. Presented at the The 28th U.S. Symposium on Rock Mechanics (USRMS), American Rock Mechanics Association.

Gale, J.F., Reed, R.M., Holder, J., 2007. Natural fractures in the Barnett Shale and their importance for hydraulic fracture treatments. AAPG Bull. 91, 603–622.

Gasda, S.E., Bachu, S., Celia, M.A., 2004. Spatial characterization of the location of potentially leaky wells penetrating a deep saline aquifer in a mature sedimentary basin. Environ. Geol. 46, 707–720. https://doi.org/10.1007/s00254-004-1073-5

Gentier, S., 1987. Morphologie et comportement hydromécanique d"une fracture naturelle dans le granite sous conrainte normale. BRGM.

Hakami, E., Larsson, E., 1996. Aperture measurements and flow experiments on a single natural fracture. Int. J. Rock Mech. Min. Sci. Geomech. Abstr. 33, 395–404. https://doi.org/10.1016/0148-9062(95)00070-4

Hansen, T.-S., Roald, S., Nomeland, T., Grant, B., 2003. Predictable and successful rock injection-the first time around A new improved system for cost-effective control of water in-leakage during tunnel excavation may reduce the need for expensive sandwich lining systems. Mater. GEOENVIRONMENT 50, 137–140.

Huerta, N.J., Bryant, S.L., Strazisar, B.R., Kutchko, B.G., Conrad, L.C., 2009. The influence of confining stress and chemical alteration on conductive pathways within wellbore cement. Energy Procedia, Greenhouse Gas Control Technologies 9 1, 3571–3578. https://doi.org/10.1016/j.egypro.2009.02.151

Jackson, R.B., Vengosh, A., Darrah, T.H., Warner, N.R., Down, A., Poreda, R.J., Osborn, S.G., Zhao, K., Karr, J.D., 2013. Increased stray gas abundance in a subset of drinking water wells near Marcellus shale gas extraction. Proc. Natl. Acad. Sci. 110, 11250–11255. https://doi.org/10.1073/pnas.1221635110

Johns, R.A., Steude, J.S., Castanier, L.M., Roberts, P.V., 1993. Nondestructive measurements of fracture aperture in crystalline rock cores using X ray computed tomography. J. Geophys. Res. Solid Earth 98, 1889–1900. https://doi.org/10.1029/92JB02298

Jorne, F., Henriques, F.M.A., 2016. Evaluation of the grout injectability and types of resistance to grout flow. Constr. Build. Mater. 122, 171–183. https://doi.org/10.1016/j.conbuildmat.2016.06.032

Krevor, S.C.M., Pini, R., Zuo, L., Benson, S.M., 2012. Relative permeability and trapping of CO2 and water in sandstone rocks at reservoir conditions. Water Resour. Res. 48, W02532. https://doi.org/10.1029/2011WR010859

Kutchko, B.G., Strazisar, B.R., Dzombak, D.A., Lowry, G.V., Thaulow, N., 2007. Degradation of Well Cement by CO2 under Geologic Sequestration Conditions. Environ. Sci. Technol. 41, 4787–4792. https://doi.org/10.1021/es062828c

Lange, D.A., Jennings, H.M., Shah, S.P., 1993. Relationship between fracture surface roughness and fracture behavior of cement paste and mortar. J. Am. Ceram. Soc. 76, 589–597. https://doi.org/10.1111/j.1151-2916.1993.tb03646.x

Luo, S., Zhao, Z., Peng, H., Pu, H., 2016. The role of fracture surface roughness in macroscopic fluid flow and heat transfer in fractured rocks. Int. J. Rock Mech. Min. Sci. 87, 29–38. https://doi.org/10.1016/j.ijrmms.2016.05.006

Massey, F.J., 1951. The Kolmogorov-Smirnov Test for Goodness of Fit. J. Am. Stat. Assoc. 46, 68–78. https://doi.org/10.1080/01621459.1951.10500769

Miltiadou-Fezans, A., Tassios, T.P., 2013. Penetrability of hydraulic grouts. Mater. Struct. 46, 1653–1671. https://doi.org/10.1617/s11527-012-0005-1

Mirza, J., Saleh, K., Langevin, M.-A., Mirza, S., Bhutta, M.A.R., Tahir, M.M., 2013. Properties of microfine cement grouts at 4 °C, 10 °C and 20 °C. Constr. Build. Mater. 47, 1145–1153. https://doi.org/10.1016/j.conbuildmat.2013.05.026

Mitchell, J.K., 1981. Soil improvement-state of the art report, in: Proc., 11th Int. Conf. on SMFE. pp. 509–565.

Müller, N., 2011. Supercritical CO2-Brine Relative Permeability Experiments in Reservoir Rocks—Literature Review and Recommendations. Transp. Porous Media 87, 367–383. https://doi.org/10.1007/s11242-010-9689-2

Neville, A.M., Kennedy, J.B., 1964. Basic statistical methods for engineers and scientists [WWW Document]. URL http://bases.bireme.br/cgi-bin/wxislind.exe/iah/online/?IsisScript=iah/iah.xis&src=google&base=REPIDISCA&lang=p&nextAction=lnk&exprSearch=167327&indexSearch=ID (accessed 11.6.17).

Osborn, S.G., Vengosh, A., Warner, N.R., Jackson, R.B., 2011. Methane contamination of drinking water accompanying gas-well drilling and hydraulic fracturing. Proc. Natl. Acad. Sci. 108, 8172–8176. https://doi.org/10.1073/pnas.1100682108

Patir, N., Cheng, H.S., 1978. An Average Flow Model for Determining Effects of Three-Dimensional Roughness on Partial Hydrodynamic Lubrication. J. Lubr. Technol. 100, 12–17. https://doi.org/10.1115/1.3453103

Renshaw, C.E., 1995. On the relationship between mechanical and hydraulic apertures in rough-walled fractures. J. Geophys. Res. Solid Earth 100, 24629–24636. https://doi.org/10.1029/95JB02159

Sanei, M., Faramarzi, L., Fahimifar, A., Goli, S., Mehinrad, A., Rahmati, A., 2015. Shear strength of discontinuities in sedimentary rock masses based on direct shear tests. Int. J. Rock Mech. Min. Sci. 75, 119–131. https://doi.org/10.1016/j.ijrmms.2014.11.009

Seidel, F.A., Greene, T.G., 1985. Use of expanding cement improves bonding and aids in eliminating annular gas migration in Hobbs Grayburg-San Andres wells. Presented at the SPE Annual Technical Conference and Exhibition, Society of Petroleum Engineers. https://doi.org/10.2118/14434-MS

Stormont, J.C., Ahmad, R., Ellison, J., Reda Taha, M.M., Matteo, E.N., 2015. Laboratory measurements of flow through wellbore cement-casing microannuli, in: 49th US Rock Mechanics/Geomechanics Symposium. American Rock Mechanics Association.

Stormont, J.C., Garcia Fernandez, S., Taha, M.R., Matteo, E.N., 2018. Gas flow through cement-casing microannuli under varying stress conditions. Geomech. Energy Environ. 13, 1–13. https://doi.org/10.1016/j.gete.2017.12.001

Tolppanen, P., Syrjänen, P., 2003. Hard rock tunnel grouting practice in Finland. Swed. Norway–Literature Study Finn. Tunn. Assoc.

Tsang, Y.W., Tsang, C.F., 1987. Channel model of flow through fractured media. Water Resour. Res. 23, 467–479. https://doi.org/10.1029/WR023i003p00467

Tsang, Y.W., Witherspoon, P.A., 1981. Hydromechanical behavior of a deformable rock fracture subject to normal stress. J. Geophys. Res. Solid Earth 86, 9287–9298. https://doi.org/10.1029/JB086iB10p09287

Witherspoon, P.A., Wang, J.S.Y., Iwai, K., Gale, J.E., 1980. Validity of Cubic Law for fluid flow in a deformable rock fracture. Water Resour. Res. 16, 1016–1024. https://doi.org/10.1029/WR016i006p01016

Zhang, M., Bachu, S., 2011. Review of integrity of existing wells in relation to CO 2 geological storage: What do we know? Int. J. Greenh. Gas Control 5, 826–840.

Zimmerman, R.W., Bodvarsson, G.S., 1996. Hydraulic conductivity of rock fractures. Transp. Porous Media 23, 1–30. https://doi.org/10.1007/BF00145263